NAGOYA UNIVERSITY

DOCTORAL THESIS

Self-identification methods of cutting-relevant information

Auther:

Kyungki Lee

Supervisor:

Dr. Eiji Shamoto

A thesis submitted in fulfilment of the requirements for the degree of Doctor of Philosophy in Engineering

In the

Manufacturing Engineering Research Group

Graduate Department of Aerospace Engineering

CONTENT

Chapter 1

Introduction

1.1 Background

Cutting is a fundamental technology to change materials into the desired shapes. It has played major roles in producing products in many fields such as automotive and aerospace industries. Since cutting is an essential process when manufacturing a tremendous number of parts, its efficiency and accuracy significantly affect the productivity and the feasibility of the entire industry; subsequently, computer numerically controlled (CNC) machine tools have been introduced. The role of CNC is to automatically execute the sequence of multi-axial motions according to the target geometry accurately. The advent of CNC machine tools has led the cutting process of the production cycle to partial automation and not only has realized a massive cut down of the costs but also has achieved high precision. However, the cutting process using CNC machine tools still has several issues that require manual operations and the decisions of experienced manufacturing engineers. For example, a precise alignment of the jigs, workpieces, and tools [1], and an observation/analysis of the undesirable phenomena such as mechanical vibrations [2,3] and tool breakage [4] are the challenging issues that require manual decision-making based on the knowledge of the cutting process. Subsequently, the process is generally planned and operated by experienced manufacturing engineers based on their skills [5]; hence automation is impeded. Nowadays, such challenges are expected to be overcome in the manner of smart manufacturing.

1.1.1 Smart manufacturing and machine tools

In the era of Industry 4.0, a concept that applies smart sensors, adaptive decision-making models, and data analytics technology into the conventional manufacturing process is suggested to achieve a further level of efficiency/quality enhancement, and perhaps the full automation in the production cycle [6,7], namely smart manufacturing (i.e., intelligent manufacturing). Even though there is no universally agreed definition of smart manufacturing, it is generally accepted as the compromisation of sensor-based data analytics, modeling, and simulation technologies from the shop floor level to the entire supply chain level along the production cycle. For example, Davis et al. define it as the dramatically intensified application of manufacturing intelligence throughout manufacturing [6]

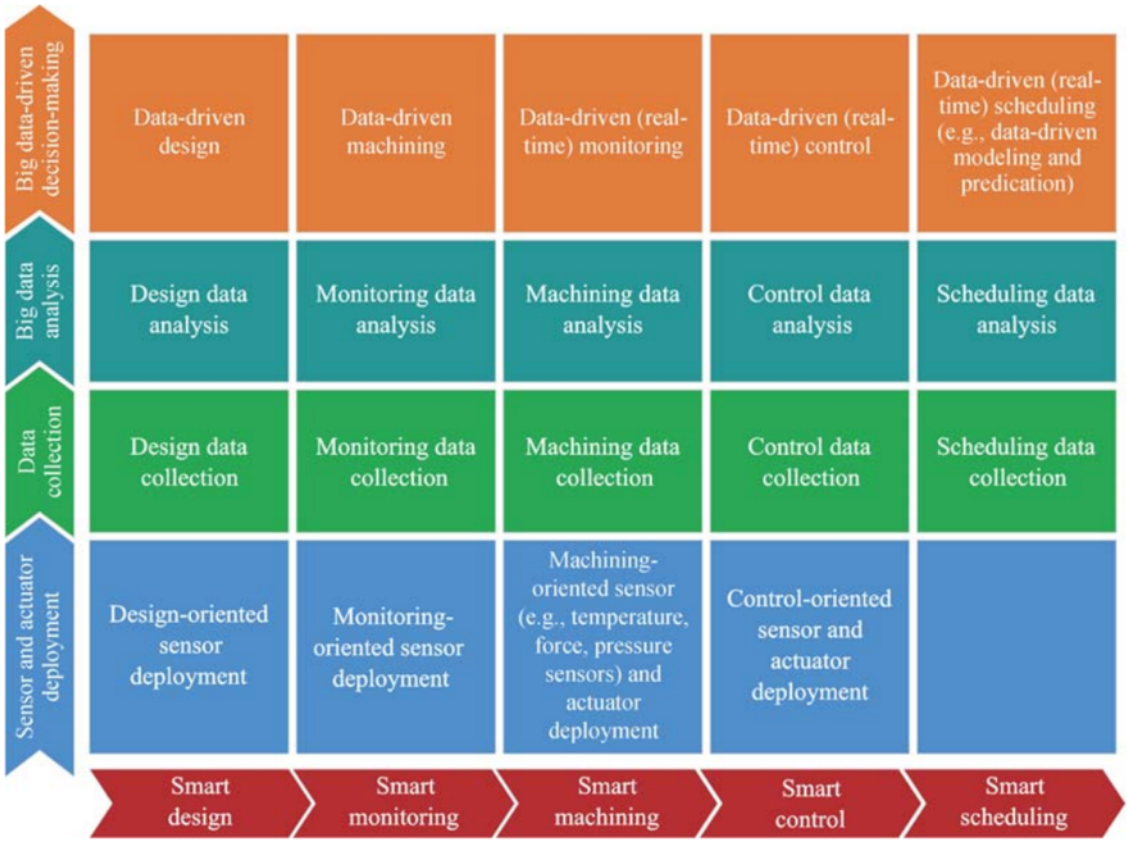

Figure 1.1. Conceptual framework of Industry 4.0 smart manufacturing systems [7].

Attempts to construct a specific model of the smart manufacturing system have been made by previous researchers. Zheng et al. suggested a conceptual framework of the smart manufacturing systems (see Fig.1.1) covering subtopics such as design, monitoring, machining, control, and scheduling [7]. Lu et al. proposed a reference model for constructing a digital twin-driven smart manufacturing system [8]. Those number of research outcomes and the existing standards [9,10] share a common concept of bottom-to-top data flow (see Fig. 1.2), which means that data are collected and integrated from local manufacturing devices, then analyzed for data-driven monitoring/optimization systems. In other words, for the realization of the smart manufacturing system in the broad scale, the information aggregation and analysis technology must be preceded at the scope of a single manufacturing device. Therefore, the research on which data is to be collected and how it is processed must be conducted first at the level of the manufacturing device.

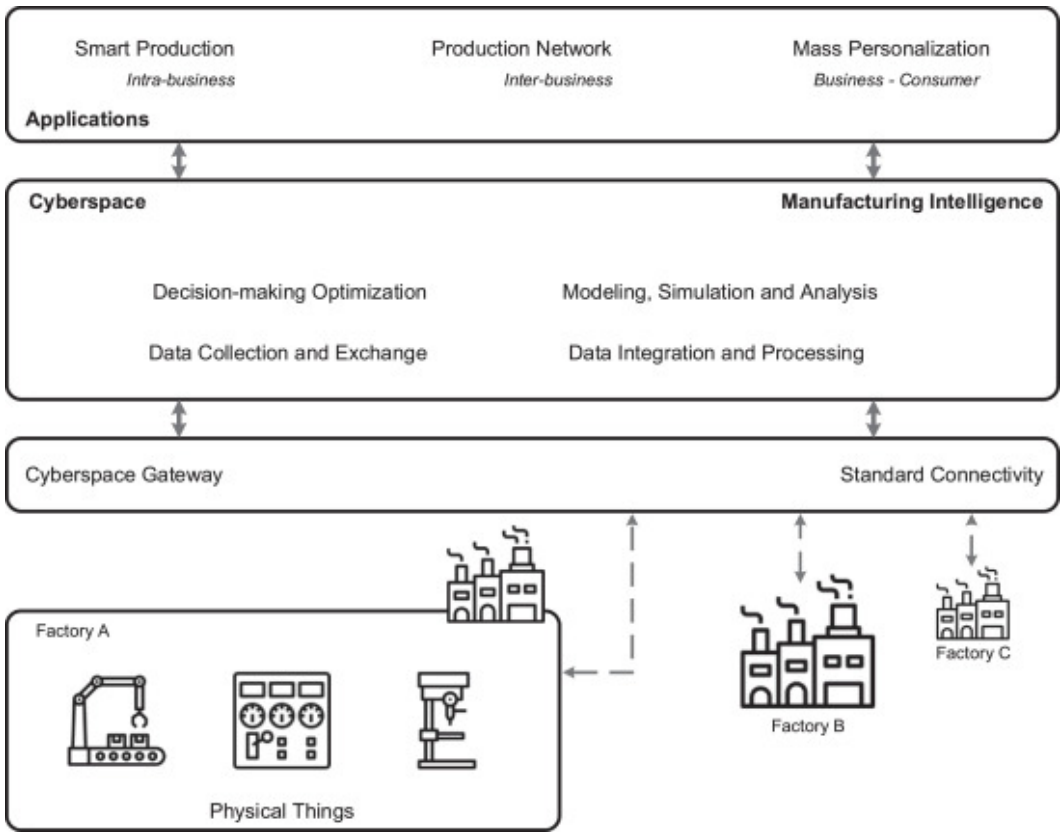

Fig. 1.2. Smart manufacturing vision [8].

In this sense, machine tools are considered as the major subtopic of the smart manufacturing system, because the cutting process is one of the key components of manufacturing. Realizing lower downtime and higher productivity by applying cutting-relevant information are the main objectives of such smart machine tools technology [11-13]. Therefore, the cutting-relevant information and its applications related to the challenges in conventional machine tool operations are being focused in this thesis.

1.1.2 Challenges in cutting process and demands for cutting-relevant information

In the following subsection, the challenging issues of machining operations are addressed in the perspective of smart manufacturing, and its relevant intelligence is explained, respectively.

1.1.2.1 Mechanical vibration

Mechanical vibrations often occur in the cutting situation. The cutting force is generally periodic in the case of the milling process, and other practical situations such as the drilling with unbalanced teeth, and the turning/boring with runout. When the natural frequencies of the machine coincide with the frequency of the periodic cutting force, the forced vibration is excited. This type of mechanical vibration has been well-known to both machine tool makers and manufacturing engineers. Generally, countermeasures are taken by simply changing the spindle rotation frequency or reducing the amount of cut during the machining process supposing the dynamics of the machine tool is given [5]. Also, other approaches such as using specially designed tools, optimizing tool postures/paths, etc., exist, but they require sufficient knowledge and skills.

Besides the forced vibration, self-excited machine tool vibrations (i.e., chatter vibration) are considered as huge obstacles because they can cause undesired tool wear/breakage, surface deterioration, and perhaps damage to the machine tools. Figure 1.3 shows examples of the chatter problem in numerous machining applications [3]. Since the stability against the chatter

vibration tends to be higher with less depth of cut, the material removal rate (MMR) must be reduced to ensure the chatter-free operation and it affects the tool-path planning. Therefore, whether the chatter vibration occurs or not, productivity significantly decreases. To clarify the mechanisms of chatter vibrations and suggest countermeasures, numerous studies were conducted throughout history and comprehensive mathematical models have been established [14-17]. Regenerative chatter vibration, the most common chatter vibration which occurs due to the regenerative effect of a chip thickness [18,19], mode-coupling chatter vibration, which occurs because of a cross-coupling of two vibrational modes existing in the plane of cut [20], and frictional chatter vibration due to the excitation effect from the contact between the flank face and the workpiece [21,22] are common types of chatter vibrations.

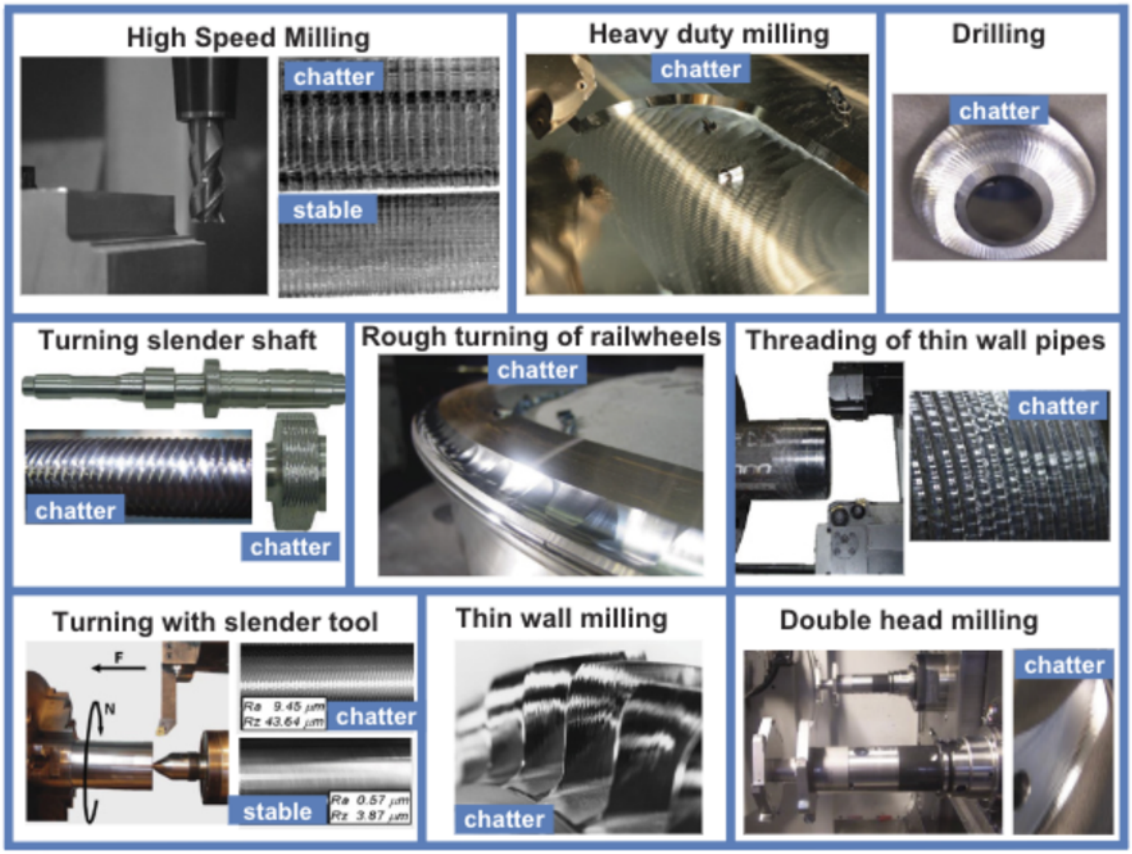

Fig. 1.3. Chatter problem in numerous machining applications [3].

Based on theoretical understandings of chatter vibrations, various countermeasures (e.g., specially designed tools [23-25], additional devices [26,27], etc.) have been proposed. Among those approaches, the most common way of avoiding the chatter vibration that is widely adopted in industrial situations is to optimize the cutting conditions such as a depth of cut (DOC) based on the stability lobe diagram (SLD) [2]. SLD, proposed by Merritt et al. [29] grounded on the work of Tlusty et al. [28], enabled prediction of the stability limit for the regenerative chatter vibration in terms of cutting parameters such as DOC and spindle speed. By selecting the optimized process parameters, maximized MMR and higher machining efficiency can be achieved without regenerative chatter vibration. The SLD method has been a critical contribution and further studies extended SLD to other machining situations (e.g., 2DoF [30]/3DoF [31] turning process, and milling process [32]). In the same manner, the stability analysis approach for mode-coupling chatter vibration has been proposed and it has been clarified that the different excitation mechanism results in different stability limit even with the same dynamics of the machine tool (see Fig. 1.4) [33,34]. This indicates that the correct countermeasure, or optimized parameter selection, corresponding to the mechanism must be chosen to avoid/suppress vibrations.

Commercial functions such as Machining Navi from OKUMA Corp., and ChatterPro from MAL Inc. were developed as a countermeasure to the regenerative chatter vibration based on the SLD method, which changes spindle speed interactively to the nearest chatter-free value when the chatter is detected, given that the dynamics of the machine tool is known. However, without the precise information of current DOC, commonly unknown in general machining operations, the thoroughly optimized spindle speed/DOC cannot be calculated in terms of MMR. Also, the excitation mechanisms must be determined beforehand. In other words, the real-time monitoring system for DOC and the dynamics, and the vibration monitoring system that can extract the information required for distinguishing the mechanism of the vibration can contribute to the realization of an automatic vibration avoidance

system.

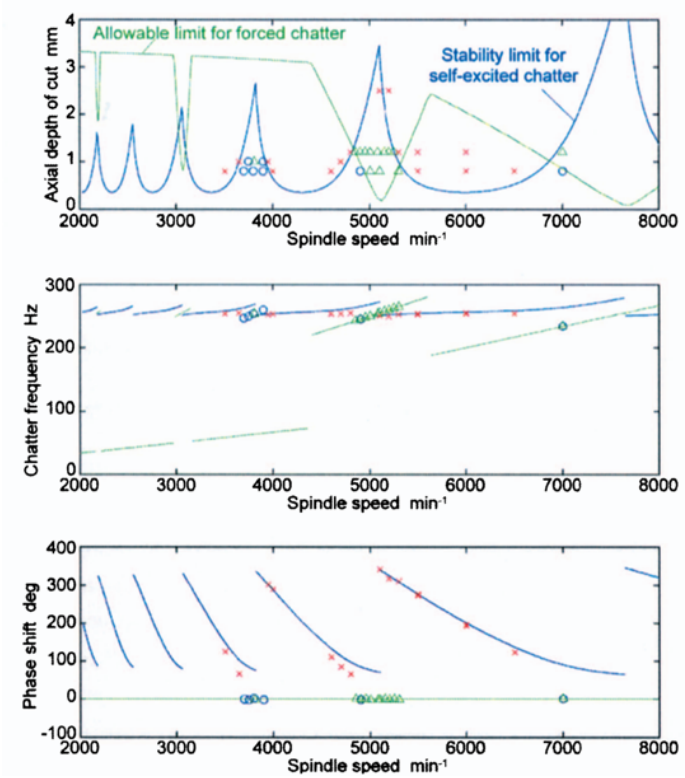

Fig. 1.4. Experimental and analytical results of chatter vibration [34]

1.1.2.2 Process geometry

The quality of a finished product depends on the geometric accuracy of the machining system since the motion of the machine tool is directly transcribed to the workpiece surface. Defined as the ability of the machine tools to produce precise 3D shapes, the measurement and the compensation strategies have been one of the major concerns of this field. Its importance is already well known to the machine manufacturers, therefore pre-diagnosis/compensation of errors such as axis errors (e.g., backlash and pitch error), shape and mounting errors of axis guiding systems, axes alignment errors and thermal errors are conducted at the stage of machine tool manufacturing [35]. Also, the concept of the volumetric calibration was introduced by previous researchers, and extensive studies have been conducted to suggest measurement/compensation schemes [36-38]. Measurement methods that measure the source of the error directly with reference materials (e.g., artifact and step gauge), and reference sensors

(e.g., interferometer) are practically utilized [39,40]. Figure 1.5 shows the example of the volumetric calibration system interface for machine tool geometry using metrology hardware [38]. However, the high cost and the installation space of metrology hardware are the current bottleneck in the industry.

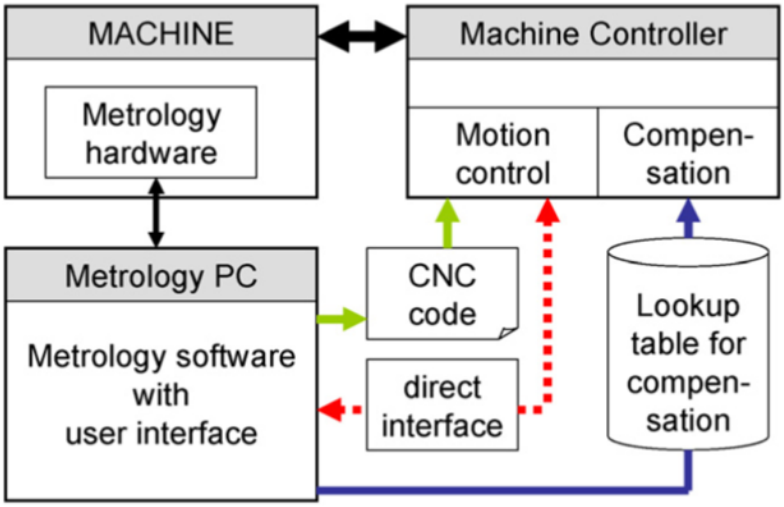

Fig. 1.5. Interfaces between the metrology for error mapping and the machine [38].

Furthermore, there remain other sources of error besides the machine tool itself, such as the tool mounting, and the workpiece mounting. Consequently, manual measurements and inspections by skilled operators and metrologists at the shop floor level are still required, even assuming the previously calibrated theoretical machine tool without any geometrical errors. Therefore, for the next generation smart machine tools, self-identification and calibration/compensation technology using information related to geometrical errors is desirable.

1.2 Motivation and objectives of the thesis

1.2.1 Motivations

Demands for monitoring cutting-relevant data to resolve the problematic issues addressed in the previous section (e.g., cutting conditions, machine tool dynamics, and process geometries) are increasing to cut down the time and economic loss. By using monitored cutting-relevant information, the manual decision-making stages for the current trial-and-error strategy are eliminated and automated, therefore higher efficiency can be accomplished throughout the machining operations. From this viewpoint, this thesis focuses on the self-identification of such useful cutting-relevant information on machine tools only with practically available data, regarding practical scenarios.

1.2.2 Research objectives

To realize the high efficiency cutting by applying cutting-relevant information, the author carried out research as follows:

1. Proposal of the DOCs and runout identification method based on easy-to-achieve information

For smart manufacturing systems, it is required to monitor the cutting process in real-time to recognize the present state of the process. Particularly, the axial depth of cut (ADOC) and the radial depth of cut (RDOC) are the key parameters when planning the vibration-free tool path with the high MMR. With the information on present ADOC and RDOC, precise predictions on the current stability margin become available, and also adequate countermeasures can be determined.

However, conventionally suggested methods for real-time monitoring of DOCs require expensive and hard-to-mount sensors, and complicated calibration processes which impede the automation. Also, they are vulnerable to vibrations occur in the cutting processes. Therefore, this research aims to propose a novel method to monitor those important

parameters (i.e., DOCs and end mill runout) in the square end milling process by analyzing frequency components of the cutting torque. Assuming efforts to predict the cutting torque using only the internal servo data by CNC tool makers and researchers in this field, the cutting torque data is expected to be available without mounting a dynamometer which is not practical [53, 54]. The proposed method assumes easily achievable information about the cutting conditions (i.e., spindle rotation speed and feed rate) and tool parameters (i.e., helix angle, nominal radius, and the number of flutes) as the given inputs. The presented method only utilizes measured cutting torque data and the given inputs; therefore, it does not require any impractical previously tuned information (e.g., specific cutting forces). In addition, an index is suggested to offer information on the reliability of the monitored outputs to the user. Graphical abstract of this research is presented in Fig. 1.6.

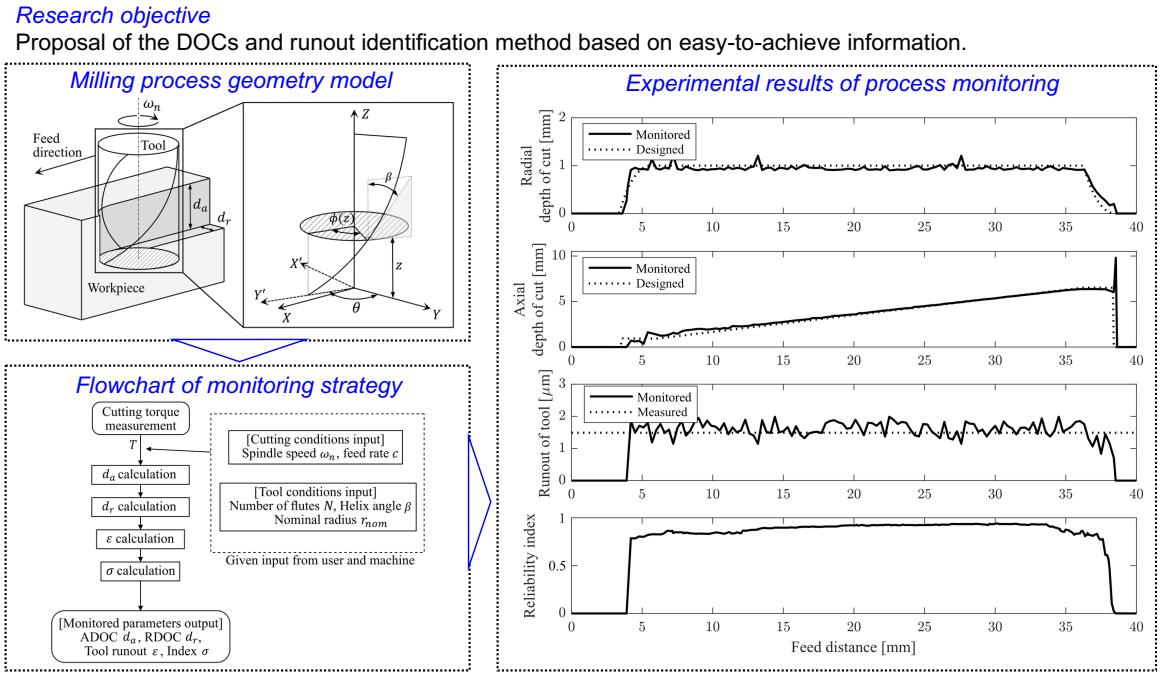

Fig. 1.6. Graphical abstract of research on DOCs and runout identification.

2. Proposal of the contact detection method based on the machine tool servo, and the rotational center self-identification method

As mentioned in the previous section, the process geometry dominates the quality of the final product. Several calibration schemes are already conducted to minimize the geometrical errors of the machine tool itself at the stage of machine tool manufacturing. However, because of the other sources of errors (e.g., tool/workpiece mounting, the inaccurate shape of tool edge, etc.) that commonly take place at the shop floor, such errors must be also considered when setting the program offsets (i.e., zero) by the operator.

The most promising way to exclude such tool/workpiece-originated errors is to attain a relative position between the tool and the workpiece. In the general turning process, solutions for attaining the tool-workpiece relative position such as in-situ touch probes, external devices mounted with air/electric micrometers, and cameras are adopted, however, they are either indirect or cost/space-consuming.

Therefore, this research aims to propose a novel direct contact detection method based on the internal data of the machine tool servo and the self-identification strategy of the rotational center as an application of the detection method. The former method compares the internal data of the non-contact and contact motions, and then precisely identifies the contact position by processing it statistically. The latter method makes multiple contacts on the pre-machined surface of the workpiece with a redundant-axis movement, and the rotational center identification is realized using the coordinates of contacts achieved by the former method. Graphical abstract of this research is presented in Fig. 1.7.

Research objective

Proposal of the contact detection method based on the machine tool servo, and the rotational center self-identification method.

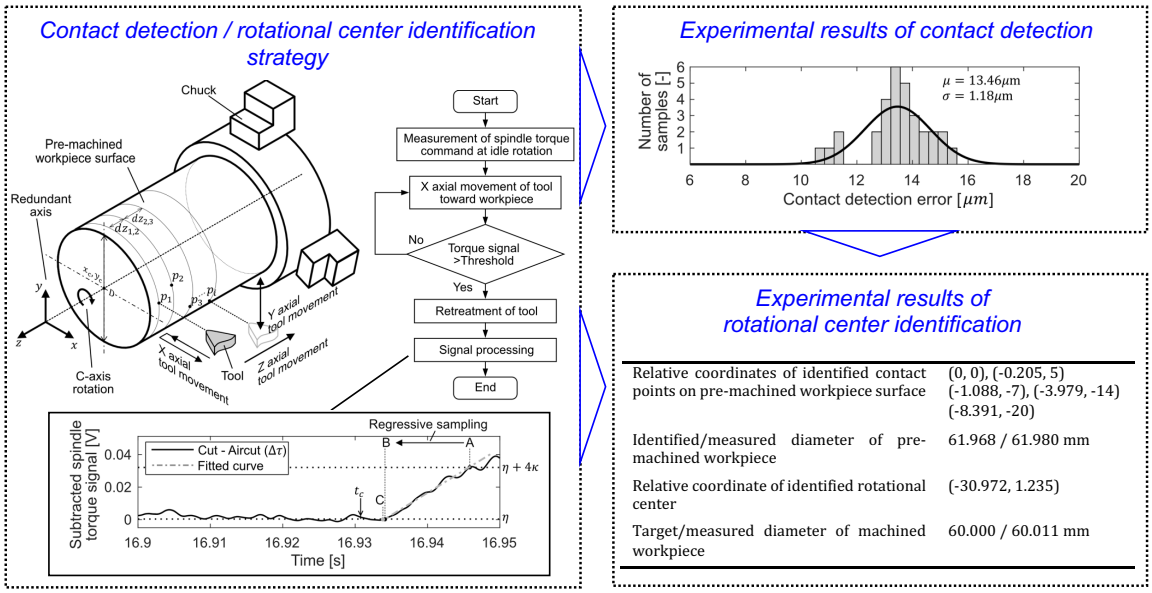

Fig. 1.7. Graphical abstract of research on contact detection and rotational center self-identification.

1.3 Structure of thesis

The present thesis consists of 4 chapters.

Chapter 1 presents the background of the smart manufacturing concept and its application to machine tool operations. Among issues of the cutting process, the mechanical vibrations and the process geometry calibration are addressed. A brief overview of studies related to such problematic issues is presented, and current counter plans and their limitations are addressed. Moreover, demands on cutting-relevant information to overcome those limitations are described in terms of smart manufacturing. The motivation and objectives of the thesis are also described, mainly on what is the desired cutting-relevant information and how it can be attained in realistic scenarios, to realize high efficiency machining.

Chapter 2 presents an identification strategy for the depths of cut and the tool runout. A novel integrated real-time monitoring method for the DOCs and the tool runout based on the frequency domain analysis of the cutting torque for the square end milling process is proposed in this chapter. The cutting torque estimation model for the square end mill process is described. Based on the analytical model, the proposed method focuses on the feature that the tool-runout-independent and the tool-runout-dependent cutting torque components are observed at different frequencies. The DOCs and the tool runout are calculated from the tool-runout-independent frequency components and the tool-runout-dependent frequency components, respectively. To offer a means for evaluating the monitored parameters to end users, a novel index is proposed, and a calculation method is presented, namely the reliability index. The results of experimental validations are presented.

Chapter 3 presents two methods for identification of the tool-workpiece relative position, specifically the rotational center, in the general CNC turning process: a novel direct tool-workpiece contact detection method and a rotational center self-identification strategy. The former method identifies the contact coordinates by utilizing the internal data of the machine tool servo.

The latter method makes multiple tool-workpiece contacts on the pre-machined surface with a redundant-axis movement. The rotational center is identified from those contacts by fitting a circle to the identified workpiece coordinates projected in the cross-sectional direction. The results of experimental validations are presented.

Conclusions of the thesis will follow in Chapter 4.

The structure of the thesis is summarized in Fig. 1.8.

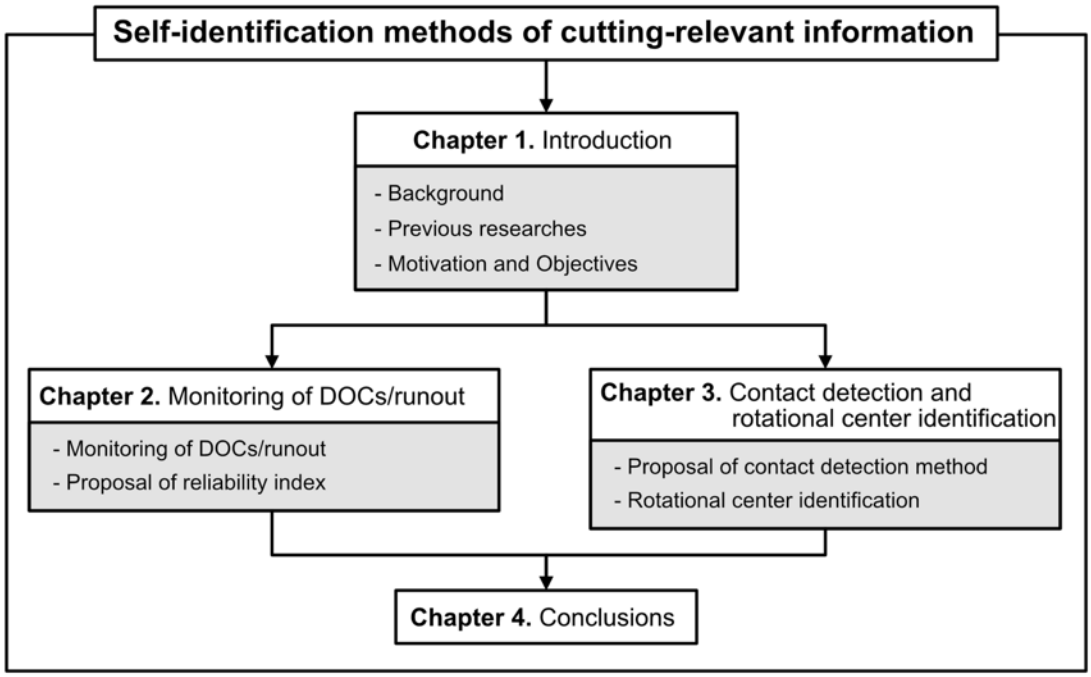

Fig. 1.8. Structure of thesis.

Chapter 2
Novel real-time monitoring method of depths of cut and runout for milling process utilizing FFT analysis of cutting torque

2.1 Introduction

The depth of cut (DOC) is a desired parameter to be monitored in the context of the smart manufacturing since it is the influential condition of the milling process. Particularly, DOC is the decisive parameter to the machine tool vibrations which limit the productivity of the milling process. Therefore, many studies focus on the DOC to avoid vibration problems [32,41,42]. The machine tool vibration is classified into several types whose generation mechanisms are different, e.g., regenerative chatter vibration, mode coupling chatter vibration [43], forced vibration [34], etc. Throughout the past studies, the basic mechanisms of these vibrations are clarified, and suppression methodologies are suggested. For the well-known regenerative chatter vibration induced by the regenerative effect, stability prediction and vibration suppression strategies are established, e.g., using the stability lobe diagram which shows the critical axial depth of cut (ADOC) [32,41,42] and critical radial depth of cut (RDOC) [43] against the spindle speed. [44]. Also, another study showed that the forced vibration can be reduced by selecting appropriate ADOC and RDOC since they have a major effect on the vibration magnitude [34]. Consequently, the information of the current DOCs is necessary for the monitoring of the current cutting status and/or suppression of general machine tool vibrations.–

Considering practical situations, the DOCs change drastically and time-by-time, e.g., near entrance/exit of workpiece, due to complicated workpiece shape, etc. Hence, the monitoring of the DOCs is difficult in the real-time and

practical situation at present, while progresses on the digital twin technologies may allow the real-time simulation of DOCs in the future. In some cases, such as the milling process having relatively simple tool paths, approaches using computer-aided manufacturing (CAM) system is valid. However, it requires the precise geometric model of the workpiece/machine tool and accurate tool paths which are not practically achievable [45]. Considering processes such as the roughing process with material bulk, this CAM approach is limited due to the inconsistent/inaccurate geometry of the workpiece. Therefore, the necessity of a real-time DOC monitoring system arises.

Various studies were conducted on the monitoring of DOCs. Prickett et al. [46] developed a monitoring system using displacement sensors mounted on the spindle. However, this method is practically unacceptable since these sensors are set in the machining environment. Gaja and Liou [47] proposed a DOC estimation method using the root mean square of the acoustic emission signal. However, a regression model and a neural network model have to be trained beforehand, and the transferability of the prediction model is yet to be studied.

On the other hand, because both the amplitude and shape of the cutting force signal in the time domain follow geometrical features of the process, numerous past approaches focused on cutting force signals to monitor the DOC [48–52]. Altintas et al. [48] estimated the DOC from the ratio of two orthogonal cutting force components in a peripheral milling process. Tarn et al. [49] focused on the tool engagement period for the estimation of the DOC. Choi et al. [50] proposed a DOC identification algorithm based on indices extracted from the cutting force shape. Yang et al. [51] also categorized types of the cutting force shapes based on geometrical relationships between the DOC and the tool shape, and indices were extracted to estimate the DOC. Leal-Muñoz et al. [52] developed a DOC estimation method for only the finishing operation based on the engagement/disengagement time of the tool. The above methods successfully monitored the DOC in various conditions. However, cutting-force-based methods introduced above either

rely on parameters which must be achieved from the calibration cut prior to the actual cutting or the shape of the cutting force which is easily affected by the vibrations and noises in practical machining. Therefore, these approaches are not adequate to solve machine tool vibration problems. Moreover, the dynamometer required to measure the cutting force signal is extremely high in cost. In addition, it limits the workpiece geometry/size and is also difficult to be used with rotational axes mounted on recent multi-axis machine tools. Therefore, relying on the cutting force signals is not desirable for the practical situation. On the contrary, efforts to predict the cutting torque using the internal servo data are recently made by researchers and CNC machine tool makers [53, 54]. Even if the prediction of the cutting torque signal from the machine tool servo becomes possible, prior studies still cannot be utilized because they require multi-directional cutting force components which cannot be observed through the cutting torque. Therefore, this Chapter presents a real-time DOC monitoring methodology that can cover the situations with the machine tool vibrations utilizing only the cutting torque signal.

Meanwhile, the cutter runout (i.e., tool eccentricity) is also a necessary parameter to be monitored in terms of smart manufacturing. Tool runout, which is the discrepancy between the rotational center and the geometrical center of the tool, causes uneven cutting loads on cutting edges and may result in deterioration of the cutting edge originated from the load concentration on certain flutes. In addition, it also affects the machining accuracy. To understand the load concentration, the effect of the runout geometry on the milling force was modeled in past studies [55,56]. These studies focused on modeling of geometrical displacements of cutter runout and the change of uncut chip thickness originated from it. Their approaches enabled the estimation of cutting forces under the occurrence of the tool runout. Based on the previous research on the cutting force models considering the effect of the tool runout, Hekman and Liang [57] developed a runout estimation method by a recursive calculation using the cutting force signals. Similarly, Seethaler and Yellowley [58] derived runout related Fourier

coefficients of multi-directional cutting forces for identification of the runout. Wang et al. [59] conducted further studies to exclude the need for the multi-directional specific cutting forces when calculating the cutter runout. However, previous runout identification approaches require process information such as the DOCs and specific cutting forces, which is usually unable to be acquired without prior calibration tests in practical manufacturing situations. In addition, the impractical dynamometer is necessary for those approaches. Therefore, demand exists for a runout monitoring method which does not require such information and device.

From these backgrounds, this research proposes a novel integrated concept of real-time monitoring method for the DOCs and the tool runout based on the cutting torque of the milling process. Besides the DOCs and the tool runout, an index that evaluates the reliability of the monitored values is also offered. The proposed approach only requires easily achievable information and does not require a calibration cut. In this Chapter, the cutting torque estimation model is first explained. Then, the monitoring method for the DOCs and the runout from the cutting torque signal is presented. Cutting/monitoring experiments are conducted to confirm the validity of the proposed method, and the results are described.

2.2 Cutting torque estimation model

2.2.1 Single-mechanism cutting torque estimation model considering runout

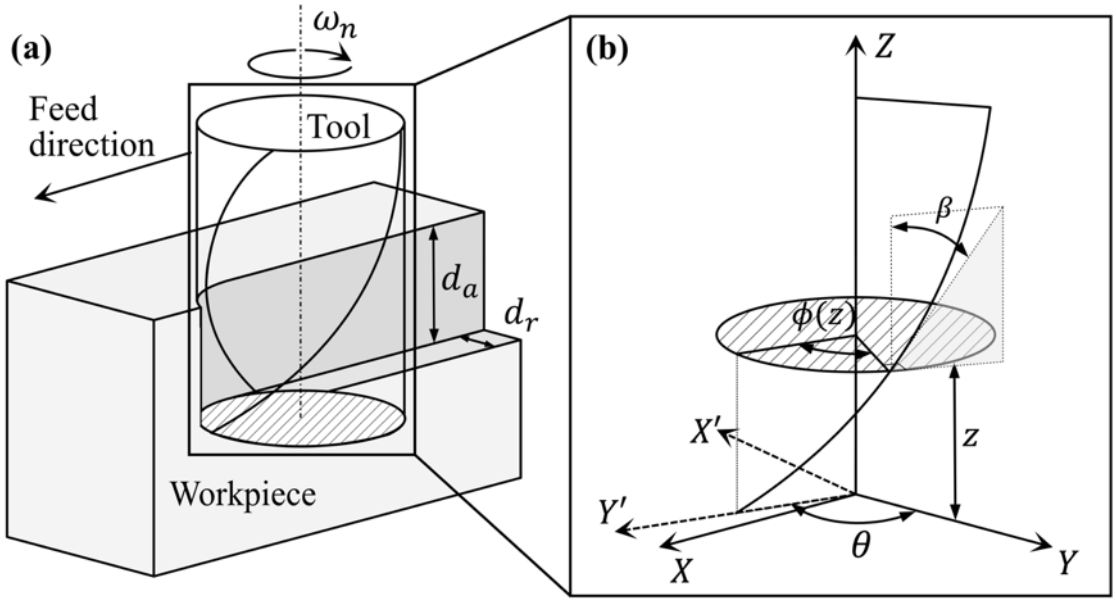

Fig. 2.1. (a) Schematic illustration of milling process and (b) Coordinate system of end mill geometry model.

By several researchers, efforts were made to predict the cutting force on rotating cutting edges based on the geometrical structure of the tool (e.g., helix angle and nominal radius) and the cutting conditions (e.g., feed rate, DOC, and rotational speed). Assuming the cutting force as a function proportional to the cross-sectional area of the uncut chip [60], cutting force prediction models can be classified into two types: single-mechanism models and dual-mechanism models [61]. Simple single-mechanism models adopt a single proportional constant, namely the specific cutting force, in which the effect of only the material removal process on the rake face is considered, where the effect of the ploughing process on the flank face during the cutting is not considered [62]. Dual-mechanism models consider the effects of the material removal process and the ploughing process separately with two independent coefficients; the specific cutting force and

the edge force coefficient [63,64]. In this study, the approach of the simple single-mechanism model is adopted for the reduction of the number of unknown coefficients. Note that the idea of the convolutional analysis of the cutting torque is inspired from the previous research of S. Y. Liang et al. [65].

Figure 2.1(a) provides an illustrative example of the milling process by a square end mill. d_r and d_a represent the radial depth of cut (RDOC) and the axial depth of cut (ADOC), respectively. As the cutter rotates with an angular speed of ω_n, the cutting edges contact the workpiece sequentially from the bottom part usually because of the helical edges. Figure. 2.1(b) shows the geometry of the tool and the coordinate systems adopted in this model, assuming that the tool has a constant helix angle of β and nominal radius of r_{nom}. $X, Y,$ and Z axes correspond to the feed, the radial, and the axial directions of the process, respectively. The positive X direction is set so that it agrees with the feed direction. The bottom edge of the reference cutting edge (i.e., the 1st cutting edge) is set to be the Y' axis. Consequently, the X' and Y' axes rotate with the tool rotation. The angular position of the i^{th} cutting edge at an arbitrary height z is calculated as follows, where θ is the rotation angle of the cutter, ϕ is the angle of the reference cutting edge at height z due to the helix (i.e., angular delay), and N is the total number of flutes. Note that the Y axis is the angular origin of θ and ϕ.

$$\phi = \frac{z \tan \beta}{r_{nom}} \tag{2.1}$$

$$\phi_i = \phi + \frac{2\pi}{N}(i-1)$$

$$\theta_i = \theta - \phi_i \tag{2.2}$$

Also, ϕ_i is the angle of the i^{th} cutting edge at height z with reference to Y' axis and θ_i is the angular position of the i^{th} cutting edge at height z with reference to Y axis.

In the practical milling process, the tool runout results in the change of the effective radii, which refers to the radii of the cutting edge trajectories under the effect of the tool runout. The geometries of the runout at the bottom

surface of the tool and height z are illustrated in Fig. 2.2. As shown in the figure, the runout displacement vector $\vec{\varepsilon}$ is defined with two variables; the magnitude of the runout, i.e., eccentricity ε, and the directional angle of it θ_{ec} in reference to the Y axis. The effective radius vector $\vec{r}_i$ of the resultant trajectory in which the i^{th} cutting edge moves along is approximated as a sum of the eccentricity vector $\vec{\varepsilon}$ and the nominal radius vector $\vec{r}_{nom,i}$ of the cutting edge. Therefore, $\vec{r}_i$ is derived as follows.

$$r_i = |\vec{r}_i| = \left|\vec{r}_{nom,i} + \vec{\varepsilon}\right|$$
$$\approx r_{nom} + \varepsilon\cos\left\{\phi + \theta_{ec} + \frac{2\pi}{N}(i-1)\right\}, \quad \text{where } r_{nom} \gg \varepsilon \tag{2.3}$$

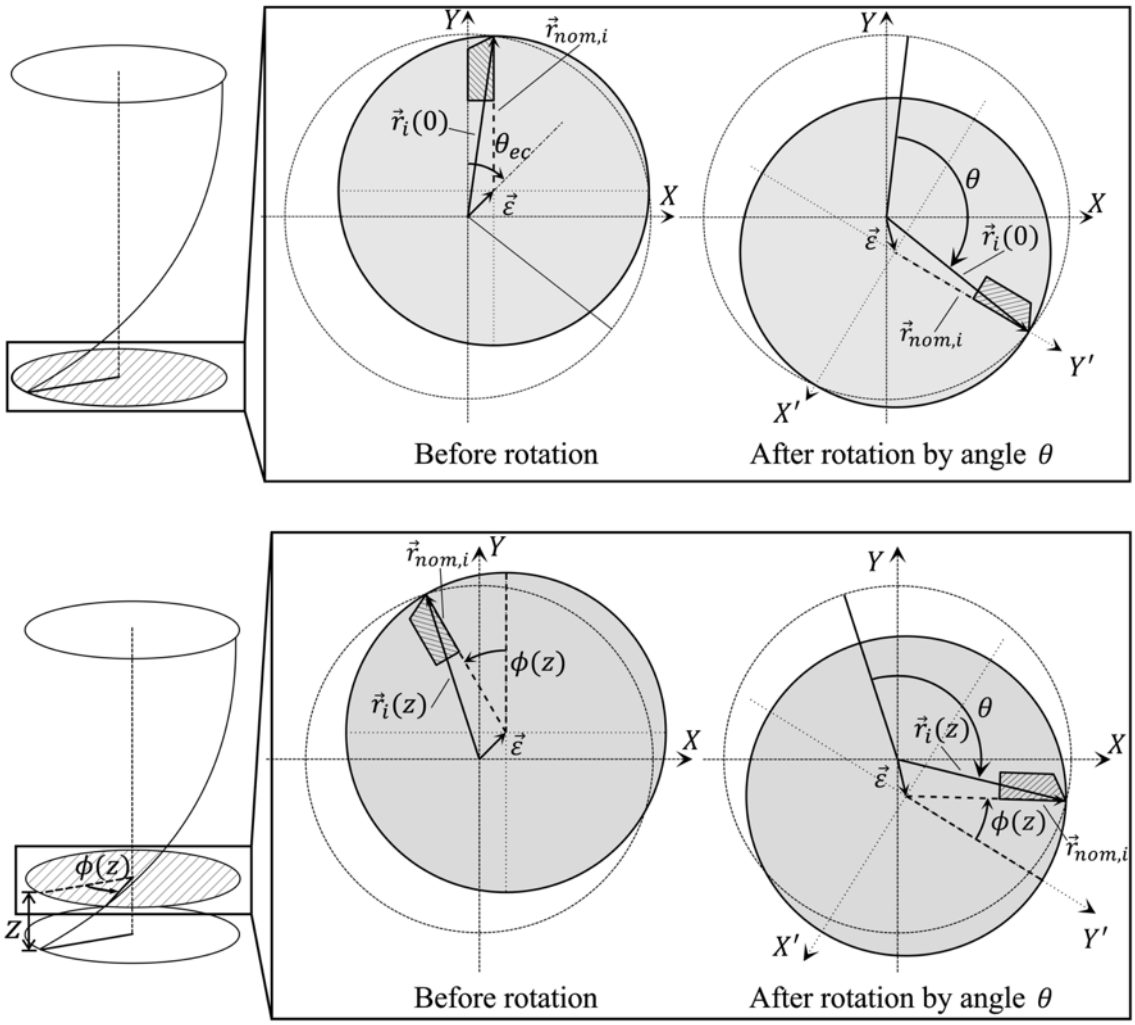

Fig. 2.2. Runout geometries at bottom and arbitrary heights.

It should be noted that the direction of $\vec{r}_{nom,i}$ depends on ϕ, and consequently r_i is a function of z. This means the radius of the resultant trajectory affected by the tool runout varies by height even in the same cutting edge (see Fig. 2.2).

As previously mentioned, the tangential component of the cutting force can be modelled as a linear function of the instantaneous cross-sectional area of the uncut chip and the specific cutting force. Figures 2.3(a) and (b) provide illustrations of the milling process without and with runout effect, respectively. c is the feed per tooth, h_i is the instantaneous uncut chip thickness of the i^{th} cutting edge, and θ_{st} and θ_{ex} are entry and exit angles of the tool immersion, respectively. Note that from the geometrical relationship, the instantaneous uncut chip thickness can be written as follows.

$$\begin{aligned} h_i &= h_s(\theta_i) + r_i - r_{i-1} \\ h_s(\theta_i) &= c\sin(\theta_i), \qquad \text{where } r_{nom} \gg c \end{aligned} \tag{2.4}$$

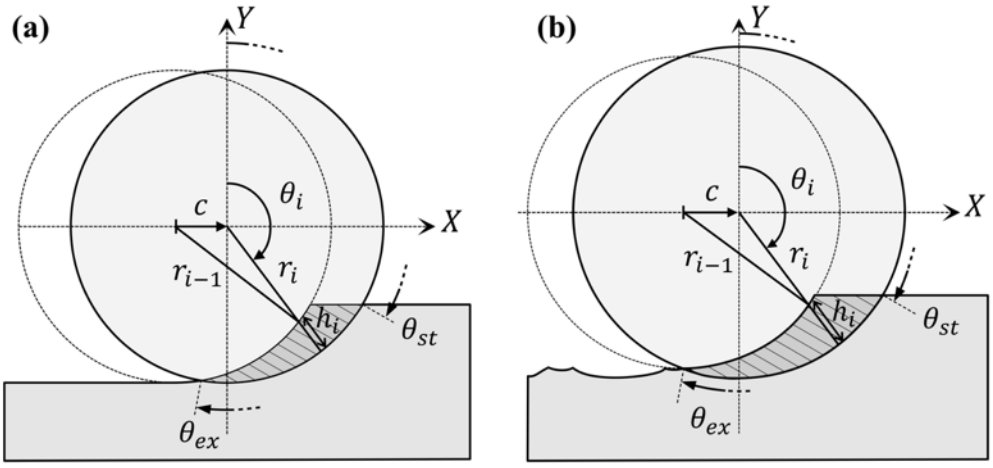

Fig. 2.3. Illustrations of milling process (a) without runout and (b) with runout.

As shown in Fig. 2.3(a), r_{i-1} and r_i are the same as r_{nom} of the tool because the runout does not exist. However, assuming the runout effect, the discrepancy between the nominal radii and the effective radii affects the instantaneous uncut chip thickness. Thus, Eq. (2.4) is transformed to Eq. (2.5) by substituting Eq. (2.3).

$$\begin{aligned} h_i &= h_s(\theta_i) + h_{ec}(\phi_i) \\ h_{ec}(\phi_i) &= -2\varepsilon \sin\frac{\pi}{N} \sin\left\{\phi_i - \theta_{ec} - \frac{\pi}{N}\right\} \end{aligned} \tag{2.5}$$

Note that the instantaneous chip thickness function for each edge can be expressed with two separate components: the chip thickness due to the rotation of the tool h_s and the chip thickness due to the tool runout h_{ec}. Because the cutting edge only engages the workpiece between the range of θ_{st} and θ_{ex}, a switch function named the tool engagement function g is employed to express the tool engagement. The range of engagement can be written as Eq. (2.6) using RDOC; a down-milling and clockwise rotation situation is written for an example.

$$\begin{aligned} g(\theta) &= \begin{cases} 1, & \theta_{st} \le \theta \le \theta_{ex} \\ 0, & \text{else} \end{cases} \\ \theta_{st} &= \cos^{-1}\left\{\frac{(d_r - r_{nom})}{r_{nom}}\right\} \\ \theta_{ex} &\approx \pi \end{aligned} \tag{2.6}$$

Strictly, the engagement range is also affected by the runout, yet it is approximated as Eq. (2.6) in this model concerning general cutting situations where ε is sufficiently smaller than r_{nom}. Moreover, the engagement range increases slightly by the relative feed motion, but this effect is also ignored since c is sufficiently smaller than r_{nom}. Based on Eqs. (2.5) and (2.6), the infinitesimal cutting force in the tangential direction and the cutting torque can be expressed as follows using the specific cutting force in the tangential direction K_t of the single-mechanism force model.

$$\begin{aligned} df_{t,i} &= K_t g(\theta - \phi_i) h_s(\theta - \phi_i) dz + K_t g(\theta - \phi_i) h_{ec}(\phi_i) dz \\ d\tau_i &= r_{nom} df_{t,i} \end{aligned} \tag{2.7}$$

where $r_{nom} \gg h_i$.

The infinitesimal cutting force function $df_{t,i}$ and the infinitesimal cutting torque function $d\tau_i$ represent the tangential cutting force and the cutting torque loaded on the i^{th} cutting edge at a discretized z plane, respectively. dz refers to the distance between the discretized planes. Therefore, the entire cutting torque loaded on the i^{th} cutting edge can be achieved by integrating the infinitesimal cutting torque in the axial direction. In Eq. (2.8), operators $*$ and $\cdot$ indicate the convolution product and the general multiplication operation, respectively.

$$\begin{aligned}\tau_i(\theta) &= \int_{z=0}^{z=d_a} d\tau_i \\ &= r_{nom}K_t\{(g \cdot h_s) * \lambda_i\} + r_{nom}K_t\{g * (h_{ec} \cdot \lambda_i)\}\end{aligned} \tag{2.8}$$

where

$$\lambda_i(\theta) = \begin{cases} \dfrac{dz}{d\phi_i} = \dfrac{r_{nom}}{\tan\beta}, & \dfrac{2\pi}{N}(i-1) \le \theta \le \dfrac{2\pi}{N}(i-1) + \dfrac{d_a \tan\beta}{r_{nom}} \\ 0, & \text{else} \end{cases}$$

λ_i, named a helical gradient function, is defined for the mathematical convenience to convert the integral operation of Eq. (2.8) in the axial direction to the angular domain. λ_i refers to the ratio of the height to the angular delay of the i^{th} cutting edge. Subsequently, the total cutting torque loaded on the entire tool can be obtained by the summation of torques acting on all cutting edges.

$$\begin{aligned}\tau(\theta) &= \sum_{i=1}^{N} \tau_i \\ &= r_{nom}K_t\left\{(g \cdot h_s) * \left(\sum_{i=1}^{N} \lambda_i\right)\right\} + r_{nom}K_t\left[g * \left\{h_{ec} \cdot \left(\sum_{i=1}^{N} \lambda_i\right)\right\}\right] \\ &= r_{nom}K_t\{(g \cdot h_s) * \lambda\} + r_{nom}K_t\{g * (h_{ec} \cdot \lambda)\}\end{aligned} \tag{2.9}$$

For convenience, let the former runout-independent term of Eq. (2.9) be

τ_s and the latter runout-dependent term be τ_{ec}. The total cutting torque can be written as follows.

$$\tau = \tau_s + \tau_{ec} \tag{2.10}$$

2.2.2 Frequency domain analysis of cutting torque

The cutting torque can be transformed into frequency components using Fourier transform. According to the convolution theorem, the convolution in the time domain is converted into simple multiplication and vice versa. Therefore, Eq. (2.10) is converted into the frequency domain as follows, where $\theta = \omega_n t$. Here, the functions of the capital letters represent the frequency domain functions which are transformed using the Fourier transform.

$$T(\omega) = T_s(\omega) + T_{ec}(\omega) \tag{2.11}$$

where

$$T_s(\omega) = r_{nom} K_t \{(G * H_s) \cdot \Lambda\}$$
$$T_{ec}(\omega) = r_{nom} K_t \{G \cdot (H_{ec} * \Lambda)\}$$

As the results of Fourier transform of Eqs. (2.5) and (2.6), functions composing the cutting torque can be described in a mathematical expressions in the frequency domain as follows.

$$\begin{aligned}
G(\omega) &= \frac{2\sin\left\{\frac{\omega}{2\omega_n}(\theta_{ex} - \theta_{st})\right\}}{\omega} e^{-i\frac{\omega}{2\omega_n}(\theta_{ex}+\theta_{st})} \\
H_s(\omega) &= \frac{1}{2} ci\delta(\omega + \omega_n) - \frac{1}{2} ci\delta(\omega - \omega_n) \\
H_{ec}(\omega) &= -\varepsilon \sin\frac{\pi}{N} ie^{-i\left(\theta_{ec}+\frac{\pi}{N}\right)}\delta(\omega + \omega_n) + \varepsilon \sin\frac{\pi}{N} ie^{i\left(\theta_{ec}+\frac{\pi}{N}\right)}\delta(\omega - \omega_n) \\
\Lambda(\omega) &= \left(\frac{e^{-i2\pi\frac{\omega}{\omega_n}} - 1}{e^{-i2\pi\frac{\omega}{N\omega_n}} - 1}\right) \frac{2\sin\left\{\frac{\omega d_a \tan\beta}{2\omega_n r_{nom}}\right\}}{\omega} e^{-i\frac{\omega d_a \tan\beta}{2\omega_n r_{nom}}}
\end{aligned} \tag{2.12}$$

Eq. (2.12) shows the Fourier transform of the functions composing the cutting torque signal. Since the mathematical model assumes the steady-state condition, the cutting torque signal is assumed as infinitely periodic. On the other hand, even though the workpiece shape changes largely, the cutting process generally changes gradually since the feed rate is small in actual situations. Hence, data processing of the cutting torque of just one rotational period can be used approximately and is also practically sufficient to monitor the cutting conditions at that moment by utilizing the introduced model. In the experiments in this chapter, the measured signal is processed period by period, which means that real-time monitoring of the cutting conditions is possible. The cutting torque can be expressed in a form of Fourier series. Then, Λ only consists of harmonic components of the tooth passing angular frequency $\omega_N = N\omega_n$ and can be re-written as a periodic impulse function.

$$\Lambda(\omega) = \begin{cases} 2\dfrac{\sin\left\{\dfrac{\omega d_a \tan\beta}{2\omega_n r_{nom}}\right\}}{\omega} e^{-i\frac{\omega d_a \tan\beta}{2\omega_n r_{nom}}}, & \omega = \pm k\omega_N \text{ where } k = 0,1,2,\cdots \\ 0, & \text{else} \end{cases} \quad (2.13)$$

Therefore, the runout-independent torque T_s is only composed of the tooth-passing angular frequency harmonics $k\omega_N$ as generally known. On the other hand, the runout-dependent torque T_{ec} is only composed of the frequency components at $(Nk-1)\omega_n$ and $(Nk+1)\omega_n$, i.e., neighboring components of the tooth-passing angular frequency harmonics. This means that T_s and T_{ec} can be observed separately of each other at independent frequency components, except for the 2-flute end mill case where the neighboring components of the different tooth-passing frequency harmonics are superimposed on each other. Therefore, the formulation for the monitoring differs between 2 flutes and more than 2 flutes.

Figure 2.4 shows a simulated example of the cutting torque for a 4-flute end mill in the frequency domain. The simulation conditions are shown in Table 2.1. As shown in the figure, T_s and T_{ec} appear independently.

Therefore, it can be concluded that parameters related to the DOCs and runout can be extracted separately from the tooth passing angular frequency harmonics and their neighboring frequencies, respectively.

Table 2.1. Simulation conditions.

Tool properties		
Helix angle β	[deg]	35
Diameter $2r_{nom}$	[mm]	6
Number of flutes N		4
Runout of tool ε	[μm]	1
Cutting conditions		
Spindle speed $60\omega_n/(2\pi)$	[min^{-1}]	1200
Feed per tooth c	[mm/tooth]	0.025
Axial depth of cut (ADOC) d_a	[mm]	1.5
Radial depth of cut (RDOC) d_r	[mm]	1.5

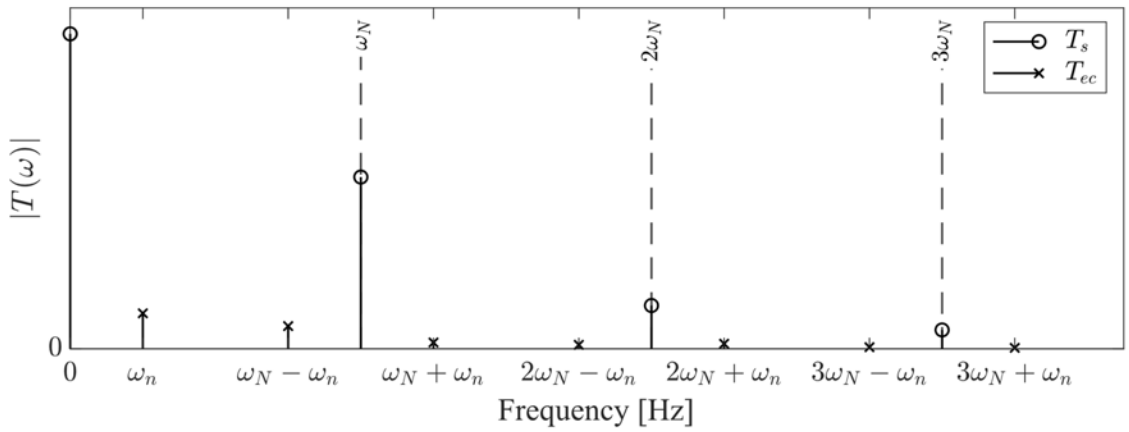

Fig. 2.4. Simulated example of cutting torque for 4-flute end mill.

2.3 DOC and runout identification

2.3.1 ADOC calculation

As previously mentioned, T_s is composed of harmonic components (i.e., integer multiples) of the tooth-passing frequency ω_N of the cutting torque T. According to Eq. (2.12), components of the cutting torque are expressed using the helical gradient function Λ, the tool engagement function G, and the static instantaneous chip thickness H_s which represent the effects of the ADOC, the RDOC, and the feed rate on the cutting torque, respectively. Therefore, the ADOC/RDOC can be monitored by calculating Λ and $G * H_s$ from T_s.

Figure 2.5(a) provides a simulated example of the amplitude of Λ. For reference, the dotted line shows the result of FFT analysis for one rotational period in infinite time domain instead of regarding the signal as periodic. The vertical lines with crosses show the frequency components of the periodic signal Λ. Note that the former one is scaled in the vertical axis to the latter one so that the crosses lie on the dotted line. As shown in this example, the frequency spectrum of Λ has periodic notches at frequencies $k\omega_{notch} = k\frac{2\pi\omega_n r_{nom}}{d_a \tan\beta}$ where $k = 0,1,2,\dots,\infty$. This is because λ is a form of a rectangular step function in the time domain, which means that the ratio of the height to the angular delay of the helical cutting edge is constant during the engagement. Since the frequency of the notches are determined by the ADOC d_a, d_a can be conversely computed by the notch frequencies estimated from the cutting torque signal. Note that $G * H_s$ shown in Fig. 2.5(b) does not have notches although G is also a step function. This is because of the convolution product operation between G and H_s. As a result, the cutting torque has notches due to the helical gradient function Λ as shown in Fig. 2.5(c). The dotted line in the figure shows the result of the FFT analysis for one rotational period in infinite frequency domain, and the vertical lines with crosses show the frequency components of the periodic signal. As shown in the figure, T_s also has multiple notches at the same

notch frequencies as Λ. Based on the idea that T_s has a notch-like shape transcribed from Λ, the nearest tooth-passing frequency around ω_{notch} is searched from the shape of the frequency components of the cutting torque. Given ω_{notch}, d_a is calculated as follows.

$$d_a = \frac{2\pi\omega_n r_{nom}}{\omega_{notch}\tan\beta} \tag{2.14}$$

Note that if d_a is close to the axial pitch of the cutting edges $d_{a,p} = \frac{2\pi r_{nom}}{N\tan\beta}$, which is the case where the $(i+1)^{th}$ tooth starts to immerse the workpiece surface as the i^{th} tooth exits, the cutting torque hardly fluctuates in the time domain. Also, ω_{notch} becomes near the tooth passing frequency. Therefore, the notch-like shape cannot be observed through harmonic tooth passing frequency components in such a case ($d_a \approx \frac{2\pi r_{nom}}{N\tan\beta}$), and only the zero-frequency component is observed. If d_a is larger than the axial pitch of the cutting edges, ω_{notch} is the same as the notch angular frequency when the ADOC is $d_a - kd_{a,p}$, where k is a natural number. Note that the integer multiples of ω_{notch} can be used simultaneously in the same manner to reduce the error of the monitoring. In this chapter, the ADOC of up to $\frac{2\pi r_{nom}}{N\tan\beta}$ is monitored by using only ω_{notch}.

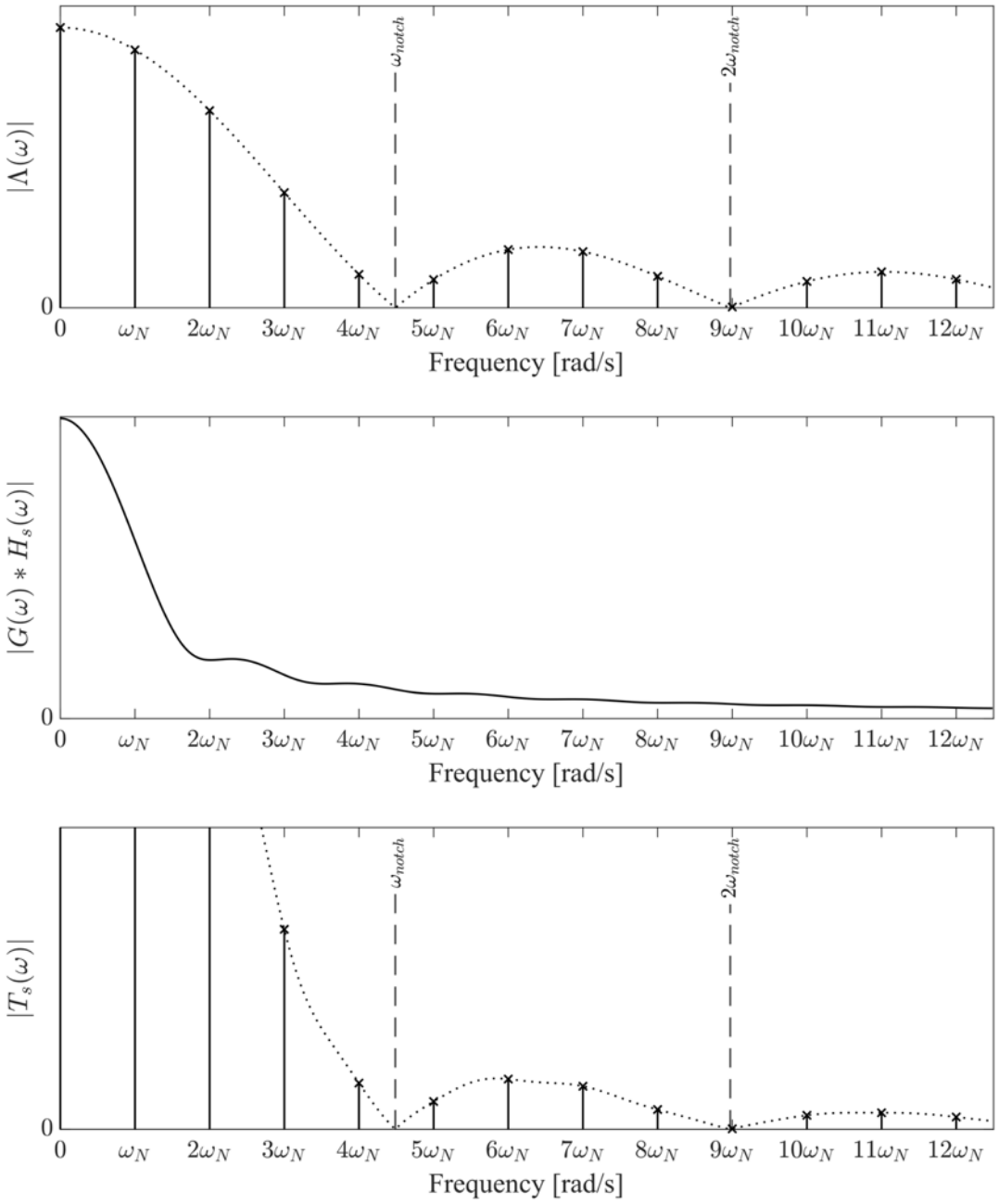

Fig. 2.5. Simulated examples: (a) amplitude of $\Lambda(\omega)$, (b) amplitude of $G(\omega) * H_s(\omega)$, (c) amplitude of $T_s(\omega) = r_{nom}K_t\{(G * H_s) \cdot \Lambda\}$.

2.3.2 RDOC calculation

Once d_a is calculated from T_s, Λ can also be estimated using Eq. (2.13). Subsequently, $G * H_s$ is calculated as follows.

$$G * H_s = \frac{T_s}{r_{nom} K_t \Lambda} \tag{2.15}$$

Although K_t is an unknown parameter, the effect of K_t can be removed by using the ratio between multiple frequency components of $G * H_s$ since K_t is common for all of the components. In this chapter, the first and the second harmonics of the tooth passing frequency are utilized for the calculation of the ratio as shown in Eq. (2.16). Note that other harmonic components can be used simultaneously to reduce the error of the monitoring.

$$\Psi \equiv \frac{G * H_s(2\omega_N)}{G * H_s(\omega_N)} = \frac{T_s(2\omega_N)}{\Lambda(2\omega_N)} \frac{\Lambda(\omega_N)}{T_s(\omega_N)} \tag{2.16}$$

Figures 2.6 and 2.7 show the relationship between the angles θ_{st}, θ_{ex} and the ratio Ψ for 1,2, and 4-flute end mills. Figures 2.6(a) and (b) show explanations and schematic illustrations of the cutting situations for each corresponding θ_{st} and θ_{ex}. Note that practical milling is conducted mostly clockwise (looking from the +z direction of a machining center), and the symmetry exists between the clockwise milling (see (i)-(iii) in Fig. 2.6) and the counterclockwise milling (see (iv)-(vi) in Fig. 2.6). Theoretically, the ratio Ψ depends on θ_{st}, θ_{ex}, and the number of flutes N; thus, θ_{st} and θ_{ex} can be calculated from the cutting torque and the monitored ADOC using the relationship provided in the figures assuming that N is given. Consequently, the RDOC is monitored using θ_{st} and θ_{ex}. In the practical monitoring process, the relationships shown in Figs. 2.7(a)-(c) are calculated beforehand and stored as lookup tables. Note that θ_{st} and θ_{ex} are independently identified prior to the RDOC. This means that the situation of up milling, down milling, and the intermediate milling process between them

can be classified, where the last one corresponds to the transient processes of the entrance/exit of the tool into/from the workpiece which occur in practical situations.

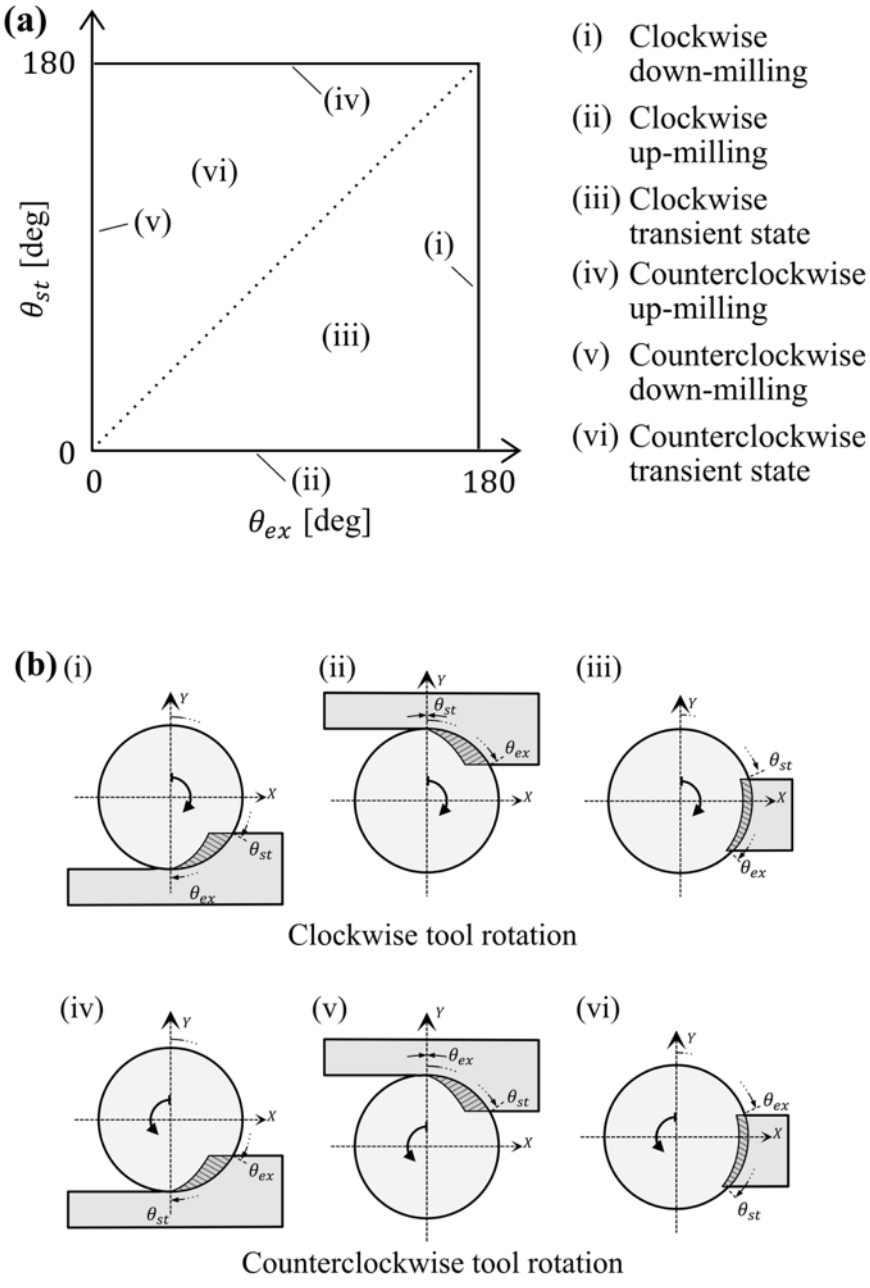

Fig. 2.6. Cutting situations for corresponding θ_{st} and θ_{ex}: (a) explanations and (b) schematic illustrations.

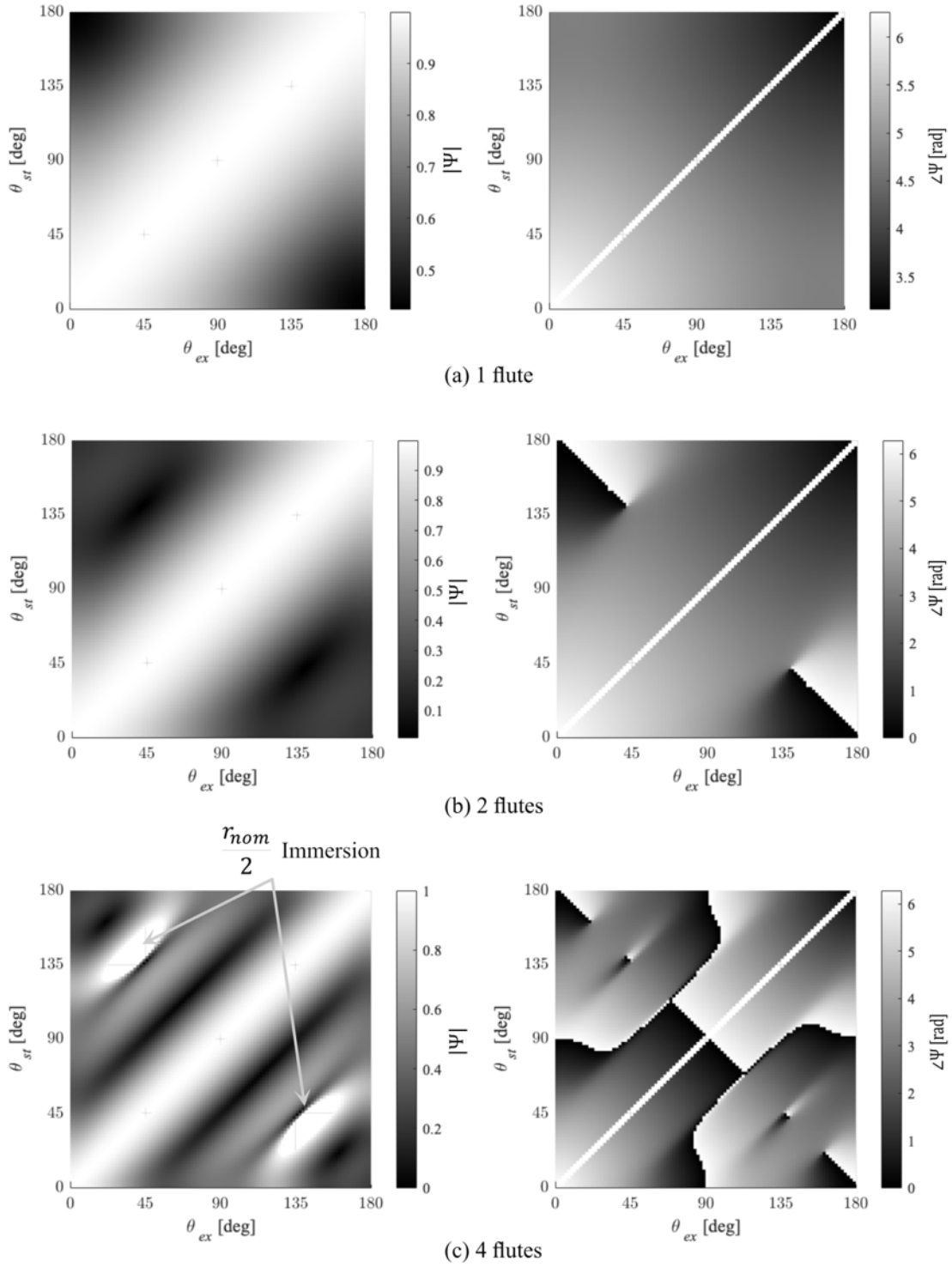

Fig. 2.7. (left) Magnitude and (right) phase of ratio Ψ.

Note that the magnitude of the ratio Ψ becomes extremely large in Fig. 2.7(c), e.g., near $\theta_{st} \approx 45°, \theta_{ex} \approx 135°$ and vice versa. The moment when the 4-flute end mill is immersed half the radius in the beginning of a slot milling process can be considered as an example. For such rare transient cases, the error of the monitoring becomes large by this calculation.

2.3.3 Runout calculation

As shown in Fig. 2.4, T_{ec} can be observed independently of T_s. In this chapter, only the ω_n component is used for the runout calculation since it is only composed of the runout-dependent torque $T_{ec}(\omega_n)$. The rotational component of the torque $T(\omega_n)$ can be derived from Eqs. (2.11) - (2.13) as follows for the case of $N \neq 1$, i.e., there is no runout for the single-flute case. Note that other harmonic components can be used simultaneously to reduce the error of the monitoring.

$$\begin{aligned} T(\omega_n) &= T_{ec}(\omega_n) \ (\because T_s(\omega_n) = 0) \\ &= r_{nom} K_t \{G \cdot (H_{ec} * \Lambda)\} \\ &= r_{nom} K_t G(\omega_n) \cdot \{H_{ec}(\omega_n) \cdot \Lambda(0) + H_{ec}(-\omega_n) \cdot \Lambda(2\omega_n)\} \end{aligned} \tag{2.17}$$

Consequently, the tool runout parameters ε and θ_{ec} can be calculated using $T(\omega_n)$ as follows from Eqs. (2.12) and (2.17) for the case of $N \geq 3$, i.e., $\Lambda(2\omega_n) = 0$.

$$\begin{aligned} \varepsilon &= \frac{|T(\omega_n)| 2\pi^2 \omega_n^2}{K_t N d_a \tan\beta \sin\left(\frac{\theta_{ex} - \theta_{st}}{2}\right) \sin\frac{\pi}{N}} \\ \theta_{ec} &= \frac{\pi}{2} - \frac{(\theta_{ex} + \theta_{st})}{2} - \frac{\pi}{N} - \angle T_t(\omega_n) \end{aligned} \tag{2.18}$$

It should be noted that d_a, θ_{st}, and θ_{ex} are already achieved from the previous monitoring steps. The remaining unknown parameter K_t can be achieved from G and Λ using Eq. (2.11) as follows. Here, only the tooth passing frequency component is utilized. Note that this specific cutting force

K_t is a useful parameter to know in practice since it reflects the effects of the tool geometry, workpiece strength, and cutting fluid.

$$K_t = \frac{T_s(\omega_N)}{r_{nom}\{G(\omega_N - \omega_n)H_s(\omega_n) + G(\omega_N + \omega_n)H_s(-\omega_n)\}\Lambda(\omega_N)} \tag{2.19}$$

For the case of $N = 2$, Eq. (2.17) can be rewritten as Eq. (2.20) using the relationship of $H_{ec}(-\omega_n) = -\overline{H_{ec}}(\omega_n)$. $\overline{H_{ec}}$ is the complex conjugate of H_{ec}, i.e., $\overline{H_{ec}} = \mathrm{Re}\{H_{ec}(\omega_n)\} - j \times \mathrm{Im}\{H_{ec}(\omega_n)\}$ where j is an imaginary unit.

$$\frac{T(\omega_n)}{r_{nom}K_tG(\omega_n)} = H_{ec}(\omega_n) \cdot \Lambda(0) - \overline{H_{ec}}(\omega_n) \cdot \Lambda(2\omega_n) \tag{2.20}$$

By comparing the real/imaginary parts of the left and right sides of Eq. (2.20), H_{ec} is calculated as follows.

$$\begin{pmatrix} \mathrm{Re}\{H_{ec}(\omega_n)\} \\ \mathrm{Im}\{H_{ec}(\omega_n)\} \end{pmatrix} = \begin{pmatrix} \mathrm{Re}\{\Lambda(0) - \Lambda(2\omega_n)\} & \mathrm{Im}\{\Lambda(2\omega_n)\} \\ -\mathrm{Im}\{\Lambda(2\omega_n)\} & \mathrm{Re}\{\Lambda(0) + \Lambda(2\omega_n)\} \end{pmatrix}^{-1} \begin{pmatrix} \mathrm{Re}\left\{\frac{T(\omega_n)}{r_{nom}K_tG(\omega_n)}\right\} \\ \mathrm{Im}\left\{\frac{T(\omega_n)}{r_{nom}K_tG(\omega_n)}\right\} \end{pmatrix} \tag{2.21}$$

Consequently, the tool runout parameters ε and θ_{ec} can be calculated as follows.

$$\begin{aligned} \varepsilon &= \frac{|H_{ec}(\omega_n)|}{\sin\frac{\pi}{N}} \\ \theta_{ec} &= \frac{\pi}{N} + \frac{\pi}{2} - \angle H_{ec} \end{aligned} \tag{2.22}$$

2.3.4 Reliability index

To evaluate the reliability of the monitored parameters, a reliability index σ is introduced. The reliability index represents the similarity between the actual frequency components and the simulated frequency components based on the monitored parameters (i.e., cutting conditions). As an example, a reliability index that mainly evaluates the reliability of the ADOC and RDOC is defined as Eq. (2.23). Here, the sum of the absolute errors between the magnitudes of the harmonic tooth-passing frequency components of the actual cutting torque signal namely $T(k\omega_N)$, and the simulated cutting torque using the monitored cutting conditions namely $T'(k\omega_N)$, is calculated. It is normalized with reference to the sum of the magnitudes of $T(k\omega_N)$ so that the cutting conditions do not affect the index, and then this value is subtracted from 1.

$$\sigma = 1 - \left(\frac{1}{\sum_{k=1}^{m} |T(k\omega_N)|} \sum_{k=1}^{m} \left| |T(k\omega_N)| - |T'(k\omega_N)| \right| \right) \tag{2.23}$$

where

$$m = \mathrm{floor}\left(\frac{\omega_{notch}}{\omega_n} \right)$$

A higher value means that the error is smaller, i.e., the monitored cutting conditions are more reliable. If the achieved cutting torque signal is noiseless and the monitoring is ideally accurate, the reliability index is 1.

Figure 2.8 shows the flowchart of the reliability index calculation step. As shown in Eq. (2.23), the reliability index is affected by the integer m, which refers to the frequency range of ratio calculation. Considering practical situations where the high frequency components of the cutting torque signal are generally small, m is set so that $m\omega_N$ is around the notch frequency of Λ in this chapter, and both the effects of ADOC and RDOC are evaluated sufficiently.

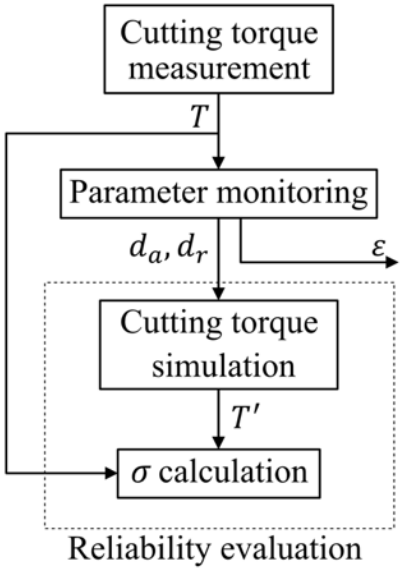

Fig. 2.8. Flowchart of reliability index calculation.

It should be noted that the reliability index cannot be interpreted directly to the errors of the ADOC and RDOC since the reliability index refers to the error of the achieved and simulated cutting torque signals. The validity is confirmed through the cutting experiments later in this chapter.

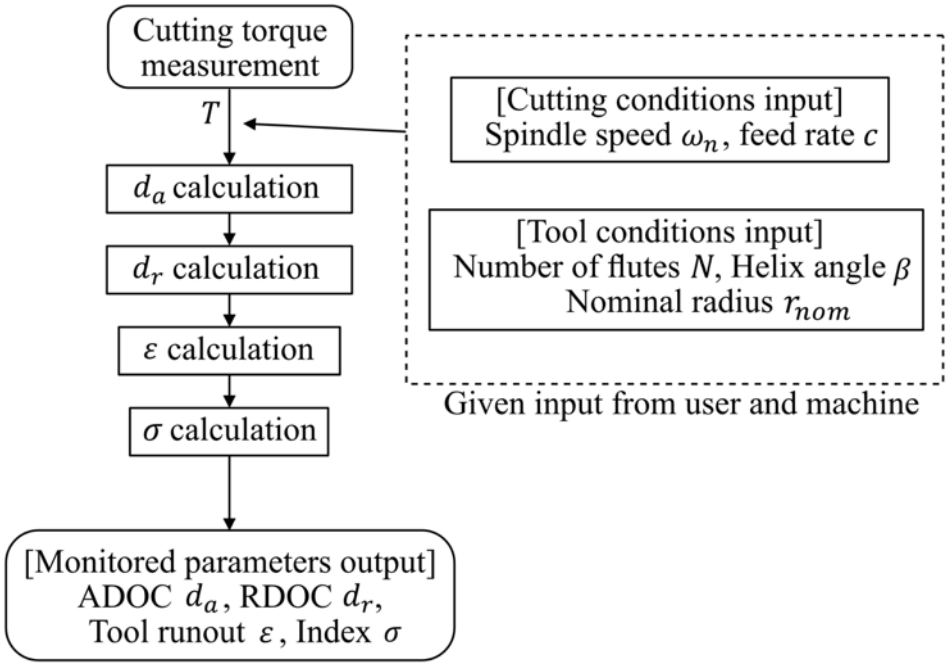

Fig. 2.9. Flowchart of monitoring strategy.

Figure 2.9 shows the overall flowchart of the monitoring strategy. Initially, the necessary information such as the spindle speed, the feed rate, the number of flutes, the helix angle, and the nominal radius of the tool are given from the user and the machine. Then, the ADOC, the RDOC, and the runout are calculated sequentially. Finally, the reliability index is evaluated.

2.4 Results and discussion

Cutting experiments to confirm the validity of the proposed monitoring method are conducted on a 3-axis machining center (SPEEDIO S500X1, Brother Industries, Ltd.). Figure 2.10 shows a photograph of the experimental setup. A typical free-cutting brass (CuZn39Pb3) is used as the workpiece, and coated 1, 2, and 4-flute carbide square end mills with a helix angle of 35 degrees are used as the tools. The experimental conditions are summarized in Table 2.2.

The z-axial cutting force instead of the cutting torque is measured with a dynamometer (9275, KISTLER) set under the workpiece. This is because the z-axial cutting force is proportional to the cutting torque for the case of the square end mill. These two data are exchangeable using the nominal radius of the end mill r_{nom} and the cutting force ratio k_z, i.e., the ratio of z axial component to tangential force. Therefore, the normalized z-axial cutting force and cutting torque can be regarded as the same and using the z-axial cutting force does not affect the logic of this proposed monitoring strategy. In the near future, the cutting torque measured/identified by the machine tool itself with sufficiently wide frequency band width may be available in practice. The magnitude of the tool runout is preliminarily measured using a dial gauge for comparison. On the other hand, the workpiece geometry after cutting is measured using a vision measurement machine (QVH4, Mitutoyo), which is sufficiently equal to the designed geometry for every experiment.

The experimental conditions can be classified into three types: constant RDOC and constant ADOC, changing RDOC and constant ADOC, and changing ADOC and constant RDOC. A schematic of each type is shown in Figs. 2.11, 2.12, and 2.13, respectively.

For the first type, both the RDOC and the ADOC of the tool path are set to be constant for a single condition as shown in Fig. 2.11, and several conditions are evaluated. The cutting experiments are conducted with the 1, 2, and 4-flute end mills. For the second type, the RDOC of the tool path is linearly increased during the cutting process whereas the ADOC is set to be

constant as shown in Fig. 2.12. The 4-flute end mill is utilized. For the third type, the RDOC is set to be constant whereas the ADOC is increased linearly along the tool path as shown in Fig. 2.13. The 4-flute end mill is utilized.

Table 2.2. Experimental conditions.

Workpiece material		CuZn39Pb3
Tool properties		
Helix angle β	[deg]	35
Diameter $2r_{nom}$	[mm]	6
Number of flutes N		1, 2, 4
Cutting conditions		
Spindle speed $60\omega_n/(2\pi)$	[min^{-1}]	1200
Feed per tooth c	[mm/tooth]	0.025
Axial depth of cut (ADOC) d_a	[mm]	0.5 - 7
Radial depth of cut (RDOC) d_r	[mm]	0.5 - 5

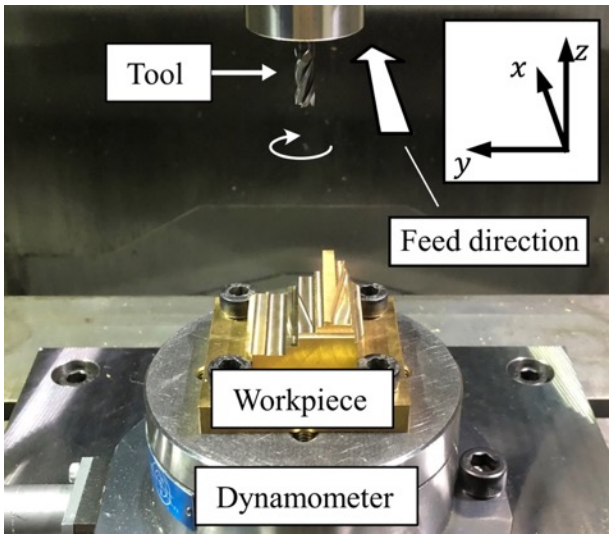

Fig. 2.10. Experimental setup.

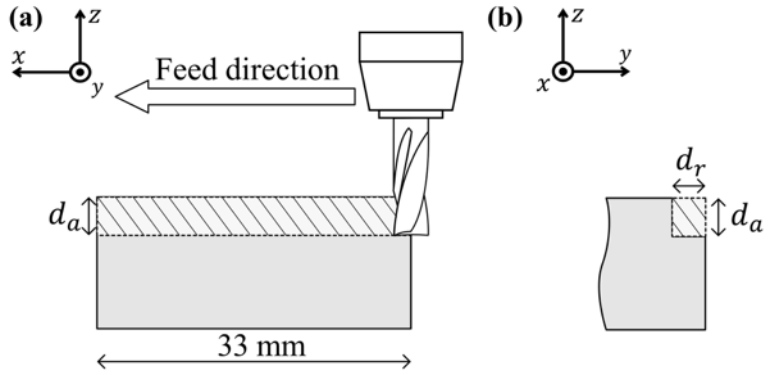

Fig. 2.11. Schematic illustration of first type of experiment: constant RDOC and constant ADOC: (a) front view and (b) side view.

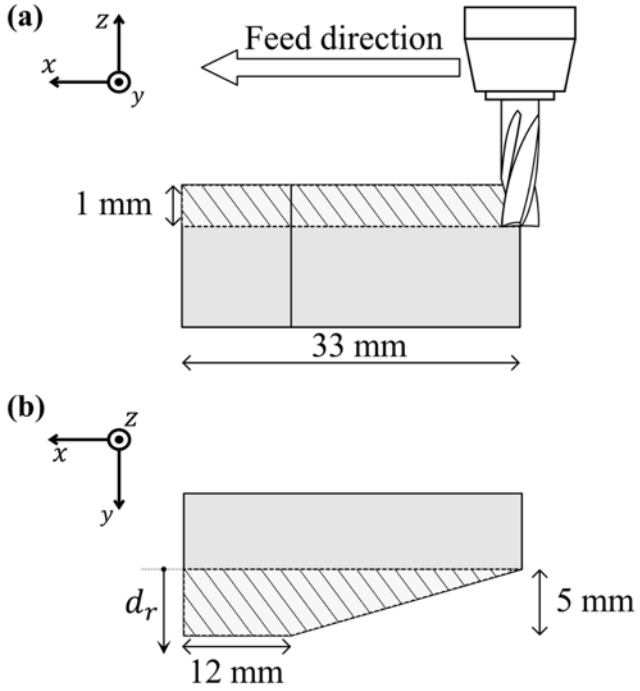

Fig. 2.12. Schematic illustration of second type of experiment: changing RDOC and constant ADOC: (a) front view and (b) top view.

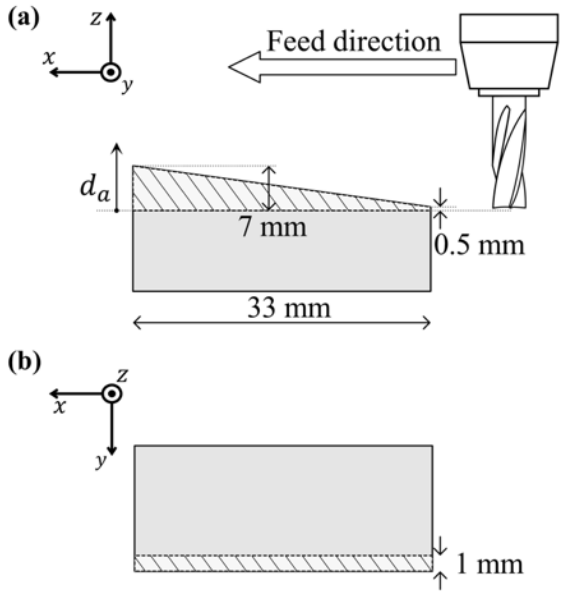

Fig. 2.13. Schematic illustration of third type of experiment: constant RDOC and changing ADOC: (a) front view and (b) top view.

The experimental results of constant ADOC/RDOC tool path are shown in Tables 2.3, 2.4, and 2.5 for 1, 2, and 4-flute end mills, respectively. The monitored values are the calculated average values throughout the tool path excluding the transient entrance/exit conditions of the tool into/from the workpiece. As shown in Table 2.3, only the RDOC and the ADOC values are compared for the 1-flute end milling processes since there is no runout for a 1-flute end mill. During the 2-flute end milling experiments, the tool has been detached and reattached; therefore, there exists a change of the runout value (see Table 2.4). As shown in the tables, the parameters are monitored, and the errors are evaluated compared to the measured values for all the cutting conditions with constant RDOC and ADOC. Figure 2.14 shows an example of the monitored data for the 4-flute end milling process with RDOC of 3 mm, ADOC of 0.5 mm, and runout of 1.5 μm. As shown in the figure, the proposed method successfully tracks each parameter.

It should be noted that the monitored runout amplitudes for the 2-flute end milling process shows greater error than the cases of the 4-flute end mill. This error is due to the additional calculation in Eq. (2.21), which is required only for the 2-flute end mill case.

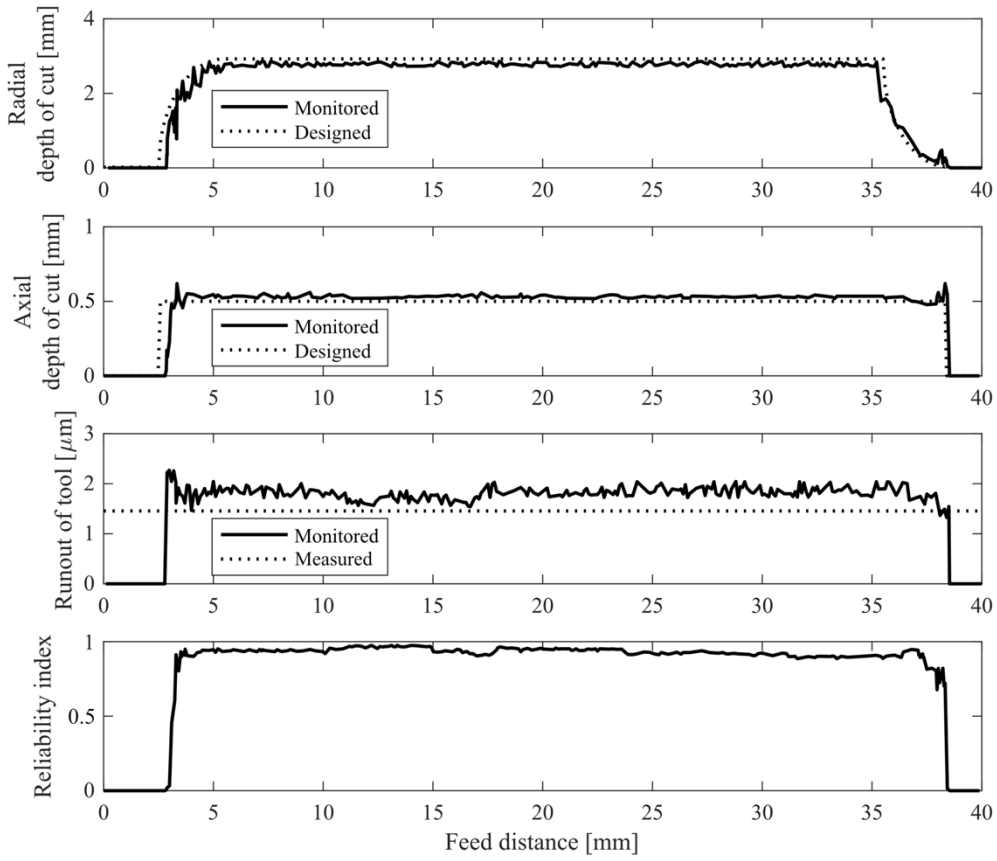

Fig. 2.14. Results of first type of experiment: constant ADOC/constant RDOC.

Table 2.3. Results of first type of experiment: 1-flute end mill.

Designed		**Monitored**		
d_r [mm]	d_a [mm]	d_r [mm]	d_a [mm]	Reliability index
1	0.5	1.223	0.466	0.88
1	0.5	0.903	0.453	0.83
2	0.5	2.113	0.473	0.91
5	0.5	5.162	0.494	0.98
0.5	2	0.601	1.921	0.93
0.5	3	0.554	2.968	0.98
0.5	5	0.725	5.441	0.90
1	5	0.798	4.632	0.89
1	2	0.946	2.041	0.97
3	2	3.179	2.176	0.88

Table 2.4. Results of first type of experiment: 2-flute end mill.

Designed		**Measured**	**Monitored**			
d_r [mm]	d_a [mm]	ε [μm]	d_r [mm]	d_a [mm]	ε [μm]	Reliability index
0.5	5	1	0.563	5.269	1.46	0.94
1	0.5		1.121	0.529	2.82	0.92
3	0.5		3.142	0.527	3	0.91
5	0.5		5.083	0.453	0.59	0.83
0.5	1	4.4	0.586	0.907	5.02	0.84
0.5	2		0.571	2.041	4.97	0.97
0.5	3		0.452	3.265	2.68	0.88
1	5		0.962	5.164	6.8	0.96

Table 2.5. Results of first type of experiment: 4-flute end mill.

Designed		**Measured**	**Monitored**			
d_r [mm]	d_a [mm]	ε [μm]	d_r [mm]	d_a [mm]	ε [μm]	Reliability index
1	0.5	1.5	1.136	0.453	1.50	0.85
3	0.5		2.924	0.51	1.71	0.97
5	0.5		5.209	0.453	1.43	0.85
0.5	0.5		0.599	0.480	1.44	0.94
0.5	1		0.524	1.134	1.28	0.87
0.5	2		0.536	2.128	1.04	0.93
0.5	3		0.51	3.080	1.19	0.97

Figure 2.15 shows the relationships between the reliability index and the DOCs error of the experimental results. The DOCs error is calculated in percentage by comparing the measured values and the monitored values. As shown in the figures, the reliability index tends to have large values when the error is small. Therefore, the reliability index can be useful information to evaluate the monitoring error.

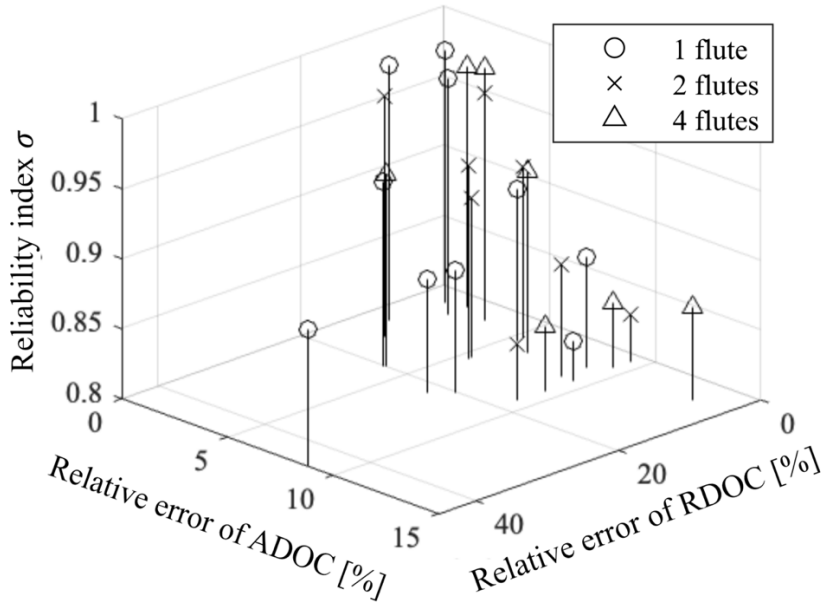

Fig. 2.15. Relationship between reliability index and relative errors.

Figures. 2.16 and 2.17 present the monitored parameters and the calculated reliability index for the second and third types of experiments, respectively. The measured runouts of the tool for both conditions are 1.5 μm. The dotted lines represent the instantaneous DOCs calculated by the workpiece/tool geometries along the feed direction. Focusing on the range where the reliability index is relatively high, the DOCs are successfully tracked even though the DOCs rapidly change in the transient states.

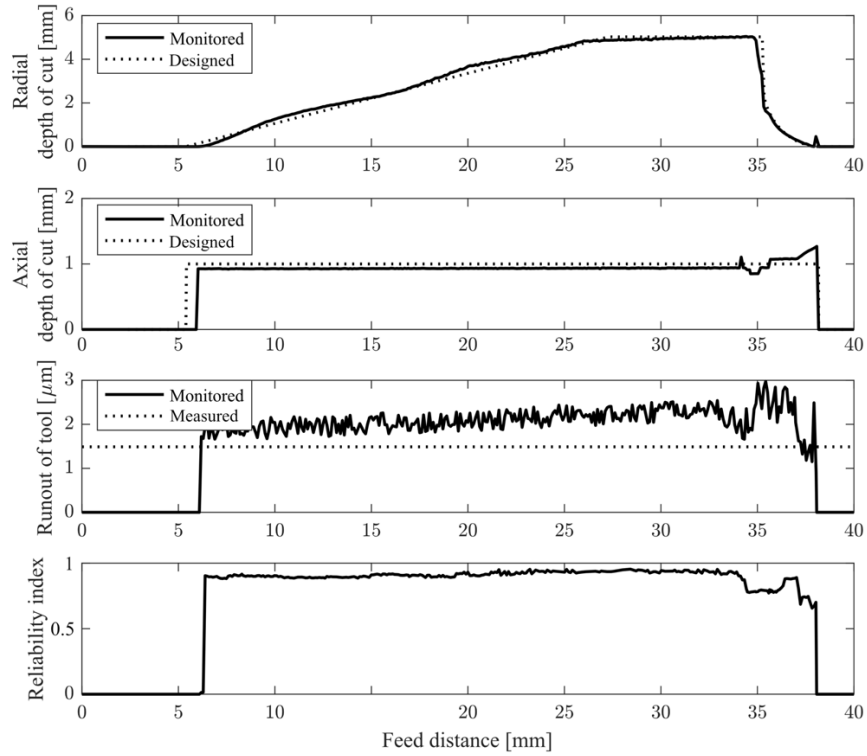

Fig. 2.16. Results of second type of experiment: constant ADOC and linearly increasing RDOC.

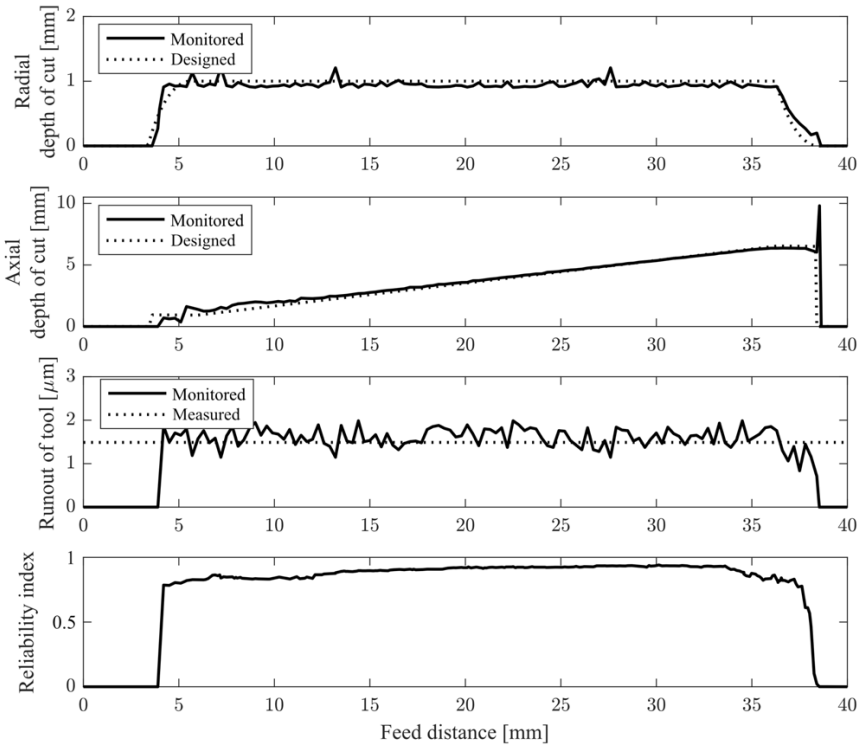

Fig. 2.17. Results of third type of experiment: linearly increasing ADOC and constant RDOC.

The above monitoring process for each tool rotation cycle is completed in under 1 ms, utilizing the developed Matlab code and a notebook computer with Apple M1 processor running at 3.20 GHz. Since the time of 1 ms spent for the proposed monitoring method for each tool rotation cycle is much less than the revolution period of the tool of 50 ms, the developed method can be executed in real-time. Also note that the sampling rate of the z-axial cutting force signal is 1 MHz which is more than enough. Considering that the sampling rate is in a trade-off relationship with the computational cost, higher execution speed is achieved by choosing an adequate sampling rate; hence, milling process with higher spindle speeds can be covered. Although the monitoring is conducted here in the timestep of the tool revolution cycle, the number of tool revolutions can be chosen flexibly, e.g., one monitoring cycle for 3 tool revolutions, on demand for the spindle speed coverage.

2.5 Summary

A novel integrated real-time monitoring method for the DOCs and the tool runout based on the frequency domain analysis of the cutting torque for the square end milling process is proposed in this chapter. The proposed method focuses on the feature that the tool-runout-independent and the tool-runout-dependent cutting torque components are observed at different frequencies. The former is observed at the integer multiples of the tooth passing frequency, and the latter is observed at the neighboring frequencies of them. Based on this feature, the notch frequency due to the helix of the tool is searched from the shape of the tooth passing frequency harmonics, and the ADOC is calculated from it first. For the next step, the RDOC is calculated using the monitored ADOC value from the ratio and phase difference between the tooth-passing frequency components of the cutting torque. With the monitored ADOC and RDOC values, the specific cutting force and the tool runout are calculated from the tool-runout-independent and tool-runout-dependent frequency components, respectively. Finally, an index for evaluating the reliability of the monitored outputs is calculated.

Experiments are conducted to confirm the validity of the proposed method. The desired parameters, i.e., the DOCs and the tool runout, are monitored from the z-axial cutting force, which is proportional to the cutting torque. 3 types of the cutting conditions, i.e., tool paths with constant ADOC and constant RDOC, constant ADOC and changing RDOC, and changing ADOC and constant RDOC, are tested. As a result, the DOCs and the tool runout are monitored successfully even for the transient conditions where the tool enters/exits the workpiece. In addition, the relationship between the suggested reliability index and the relative errors of the DOCs is investigated. The index is shown to be correlated with the monitoring error of the DOCs; therefore, it can be said that the introduced index indicates the reliability of the monitored parameters.

Chapter 3
Novel rotational center self-identification method of machine tool by utilizing multiple tool-workpiece contacts with redundant-axis movement

3.1 Introduction

In the general CNC turning process, the dimensional accuracy of a finished product strongly depends on the relative position between the workpiece and the tool set by the user. Therefore, its identification, e.g., the relative vector from the rotational center of the workpiece to the cutting edge, has to be conducted precisely. Conventionally, the relative position between the workpiece and the cutting edge is identified by slightly cutting the workpiece within the finishing allowance and measuring its diameter manually; automation is impeded.

To realize automation, the method using touch probe sensors or tool setters are commonly adopted to the practical CNC turning process [66]. However, since the position of only the tool is measured, the positional error of the rotational center is included; preciseness lacks. On the other hand, this error can be excluded by feedbacking the diameter error of the machined workpiece measured by an external machine mounted with air/electric micrometers [67]. However, this is an ex-situ method [68], i.e., it is not capable of immediate compensation, and additional equipment is necessary [69]. For this concern of the downtime loss of the machine due to the ex-situ scenario, several in-situ workpiece measurement methods based on mounting various types of sensors on the machine are suggested [70-72]. Still, these methods require precise alignment of the sensors and the additional costs due to the installation of the sensors. Consequently, an in-situ method to identify the diameter error without additional equipment is

desired.

Meanwhile, in the author's understanding, there has been no research to realize machine tools which can self-identify their machining errors, e.g., diameter error, without additional sensors and/or precise reference surfaces. However, the author have realized that such self-identification becomes possible by utilizing multiple direct contacts between a tool and a pre-machined workpiece surface with redundant-axis movement of recently available multi-axis machine tools, e.g., turning centers equipped with a Y-axis, since number of these machine tools has increased in the market for process consolidation in shops. For example, the rotational center coordinates and the diameter of the workpiece in turning can be smartly identified, which can be used for future automation.

In order to realize the above smart self-identification strategy, a precise detection method for the direct contact between the tool and the workpiece is required, which is analogous to the touch probe method but uses the tool edge instead of the touch probe. Precedent researchers suggested a variety of such direct approaches. Machine-vision-based and optical approaches are commonly utilized for commercial usage; however, they require a precise sight alignment [68], which is undesirable. On the other hand, several researchers reported acoustic-emission-sensor-based contact detection methods [73-77]. In addition, Castaño et al. proposed a conductance-sensor-based method targeting conductive materials [78]. Nevertheless, equipping external sensors to the machine tools is cost/space-consuming and fragile in a machining environment. Meanwhile, a sensor-less method utilizing a disturbance observer of the internal servo system is proposed as an alternative to the above sensor-based methods [79]. Concerned with the precision of the contact detection, the above studies [73-77,79] reported that they successfully detected the tool-workpiece contact under sub-micron order error for precision machining. However, they rely on the high positioning resolution of precision machine tools, which is at least ten times higher than general machine tools. Therefore, the above methods are not suitable for the scale of the general CNC turning process. In addition, their

threshold-based judgment of the contact state from the signals contains an error because of the delay from the actual and precise contact timing.

From these contexts, this study firstly proposes a direct tool-workpiece contact detection method by utilizing the internal data of the machine tool servo for the general CNC turning process. The threshold-originated-error is excluded by processing the time-sequential internal data regressively. Furthermore, servomechanism-originated-error is excluded by comparing the data of non-contact and contact motions. Secondly, the rotational center self-identification strategy based on multiple tool-workpiece contacts on the pre-machined surface with a redundant-axis movement is proposed. The pre-machined workpiece surface is regarded as a cylindrical shape centered on the rotational center of the machine, and the workpiece profile can be identified from multiple contact points by fitting a circle to the workpiece projected in the cross-sectional direction. Then, experimental results of the contact detection are presented. Lastly, an outer diameter turning experiment is conducted to confirm the validity of the rotational center identification method.

3.2 Concepts of proposed method

Two methods are proposed in this research: precise contact detection and rotational center identification. Figure 3.1 provides a schematic illustration of the proposed methods. p_i refers to the i-th contact point used for the rotational center identification, and $dz_{i,i+1}$ refers to the Z-axial distance between the i-th and the $(i+1)$-th contact points. In the former method, the moment of contact is identified by processing the time-sequential internal data backwardly. In the latter method, the redundant-axis movement, specifically referring to the Y-axis in this research, is utilized so that multiple contacts are made on the pre-machined surface. Using the information extracted by these contacts, the workpiece profile, including the rotational center, is identified. The detailed concepts of the proposed methods are explained as follows.

3.2.1 Contact detection method

The proposed contact detection method involves a two-step sequential motion of the machine tool; an aircut motion and a cut motion. Here, the aircut/cut motion refers to a rotation without/with a radial feed-axis (X-axis) movement of the tool, respectively. The same spindle movement is commanded for both motions.

Figure 3.2 shows the flowchart of the contact detection. First, the spindle servo data, namely the spindle torque command signal in this research, during the aircut motion is achieved. Then, during the cut motion, the tool is fed along the X-axis and contacts the workpiece surface with a bit of removal of the workpiece material within the finishing allowance; accordingly, the torque command signal of the spindle servo arises following the ploughing/cutting force (i.e., contact force). Afterwards, the tool retreats.

Under the assumption that the torque command signal of the aircut motion shows sufficient repeatability, e.g., torque ripples corresponding to bearing kinematics and cogging torque, the influence of the contact force on the torque command signal can be observed by comparing the cut motion to

the aircut motion. In other words, the torque command signal of the previously recorded aircut motion is subtracted from the signal of the cut motion. The exact moment of the contact is identified by processing the subtracted signal. Then, the rise of this subtracted signal due to the contact is sampled backward from the moment when it exceeds the set threshold to the moment when it falls below the mean value of the idle-rotation state. The sampled data is fitted by a regression line/curve, specifically a regression line in this research. Subsequently, the moment of the intersection between the fitted line and the mean value of the idle-rotation state is identified to be the exact moment of the initial contact. The positional signal of the X-axis servo is achieved during the cut motion; thus, the coordinate of the contact point can be obtained. The detailed signal processing method including the selection of the threshold value is explained with a numerical example in the further part of this chapter (see Chapter 3.2).

Note that the repeatability of the torque command signal of the idle rotation is important; thus, the influence of the mechanical structure (e.g., positions of bearing rollers and rotor) inside the spindle should be considered. For this purpose, the C-axis is rotated in the counter direction to initialize the spindle position after the aircut. For example, if the C-axis is rotated 90 degrees for the aircut motion, it is rotated -90 degrees before starting the cut motion.

3.2.2 Rotational center identification

Suppose a cylindrical workpiece is mounted on a typical 4-axis (X-Y-Z-C) CNC lathe, where the Y-axis is necessary for the rotational center identification. The workpiece is pre-machined without the accurate information of the rotational center; therefore, the diameter is unknown, but the pre-machined surface can be regarded as a cylindrical shape centered on the rotational center of the spindle. Figures 3.1 and 3.3 provide schematic illustrations of the proposed rotational center identification method. A basic circle fitting based on least squares method is utilized here [80]. As shown in the figures, contacts are made at multiple points (minimum of 3 points

including the point where the pre-machining was conducted, but more points are recommended for the accuracy of the identification; discussed later in this chapter) at different Y-axis, namely redundant-axis, positions. To avoid the overlapping of contacts, the Z-axis positions may be also moved slightly for each contact. Since the Y-axis is the redundant-axis, which is independent of the pre-machining, the diameter of the workpiece and the rotational center coordinates can be attained by fitting a circle in the X-Y plane with the calculated contact coordinates on the cylindrical surface. In this research, the coordinates of the contact points are acquired using the proposed contact detection method, and the circle is fitted by the Gauss-Newton algorithm.

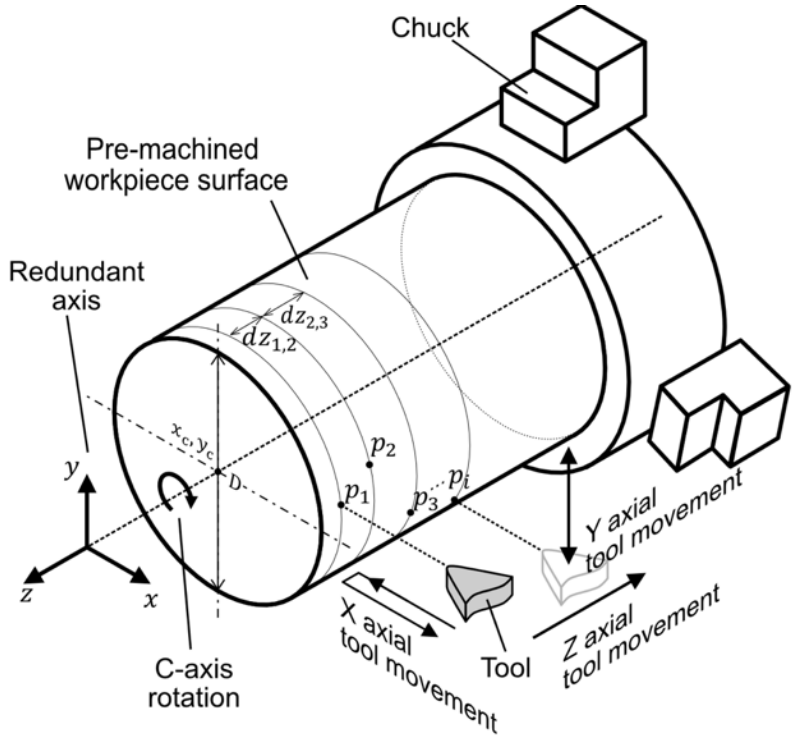

Fig. 3.1. Schematic of contact detection and rotational center identification.

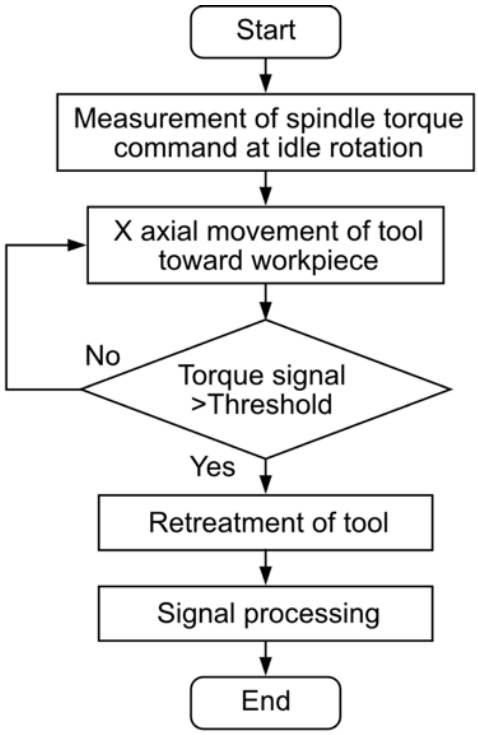

Fig. 3.2. Flowchart of contact detection.

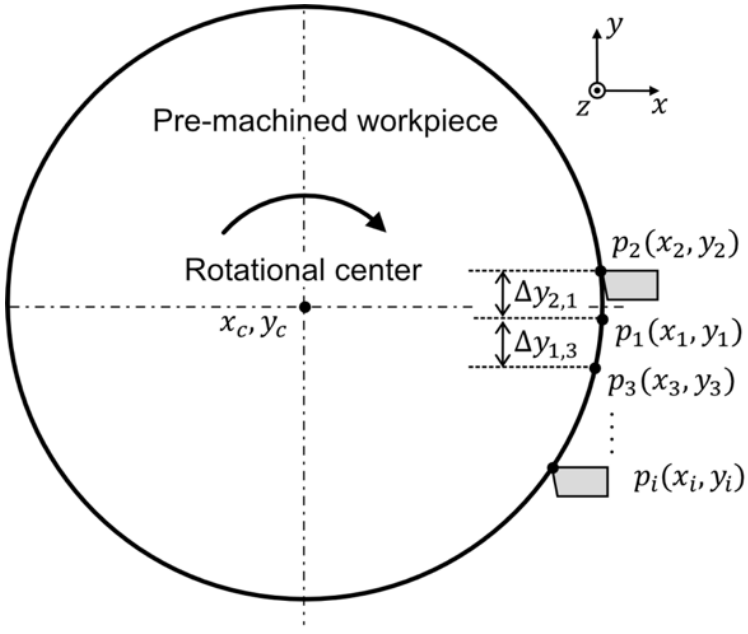

Fig. 3.3. View in Z-axis during rotational center identification.

3.3 Data processing

3.3.1 Experimental setup

The contact detection experiment and the outer diameter turning experiment are carried out to confirm the validity of the proposed methods. Figure 3.4 shows a photograph of the experimental setup, and Table 3.1 shows the experimental conditions. A CNC lathe (Okuma Corp., SPACETURN LB3000EX) is utilized, and a tool insert (Mitsubishi Material Corp., TCMW16T308 HTi10) mounted on a tool shank (Steel, ISO C45) is used to contact a cylindrical workpiece (Brass, ISO CuZn39SN1). The contact detection experiment is conducted with a workpiece diameter of 68 mm, and the outer diameter turning experiment is conducted with a diameter of 62 mm.

To ensure enough repeatability of the spindle torque command, the workpiece is rotated a total of six turns for each aircut/cut motion. After five preliminary revolutions, the tool is fed toward the workpiece for the cut motion from 5 mm above the surface to a depth of cut of 0.1 mm, and then it is pulled back to the initial position.

For the contact detection experiment, the set of the aircut and cut motions is conducted 30 times so that enough samples to evaluate the proposed method can be obtained. The X/C-axes are controlled simultaneously for the contact detection here. The contact position is calculated using the proposed method from the obtained servo signals. Since the workpiece is pre-machined, the X-axis and Y-axis positions of the pre-machining process, namely x_{true} and y_{true}, are regarded as the true contact coordinates. The Y-axis position of the 30 aircut and cut motions is unchanged from that of the pre-machining, i.e., y_{true}; thus, the errors of the proposed contact detection method are evaluated by comparing the detected X-axis positions of the contacts with x_{true}. To avoid the overlapping of contacts, which can affect the preciseness of the contact detection method, the Z-axis position is moved slightly for each contact. Note that y_{true} is a roughly set value without the knowledge of the precise position of the

rotational center.

Afterwards, the outer diameter turning experiment is conducted to confirm the validity of the rotational center identification method. 5 points at different Y-axis positions, ranging from $y_{true} - 20\,mm$ to $y_{true} + 5\,mm$ in this experiment, are utilized. Since the position of the pre-machining process is regarded as the known true contact coordinates, 4 additional contacts are made. Note that this Y-axis position range is selected to be nearly the maximum extent while avoiding the flank face interference; thus, the Y-axis position range is dependent on the tool insert shape and the roughly known diameter. Note also that only one contact is made for each Y-axis position. Using the positional information extracted from these contacts, the rotational center is identified. Next, the workpiece is turned to the set target diameter using the identified rotational center, and the diameter of it is measured with a micrometer. The error between the target and measured diameters is evaluated.

3.3.2 Contact detection processing

Figure 3.5 shows an example of the achieved servo signals. $\tau_{air}(t)$ and $\tau_{cut}(t)$ refer to the torque command signals of the aircut and cut motions, respectively. Note that the difference of the torque commands at the beginning has no essential meaning since the C-axis control is off, and the reason of the counterclockwise rotation of the spindle near the end of the signal is to initialize the spindle position for the next contact, see Section 2.1. If the exact moment of the contact is given as t_c, which can be identified from x_{true}(true contact coordinate) and the X-axis position signal, it can be observed that τ_{air} and τ_{cut} have sufficient repeatability for $t < t_c$ (see Fig. 3.5(c)). The difference between the torque commands of the aircut and cut motions starts to appear as the tool begins to contact the workpiece surface. Note that the rise of τ_{cut} itself by the contact can hardly be judged (see Fig. 3.5(b)); hence, the signal of the air cut motion and its subtraction is essential for the precise contact detection in standard-accuracy machine tools.

Figure 3.6 shows an example of the subtracted signal $\Delta\tau = \tau_{cut} - \tau_{air}$.

Let t_0 be the time when the spindle starts to rotate and T be the cycle time of rotation. η and κ refer to the mean and the standard deviation of $\Delta\tau$ for $t_0 + 4T \leq t < t_0 + 5T$, respectively. In other words, they are calculated during the rotation just before the tool starts to be fed. When $\Delta\tau$ reaches a set threshold of $\eta + 4\kappa$, namely point A in the figure, it is sampled backward from point A to the point where it first reaches η, namely point B. Then, a straight line is fit against the rising signal of the section A-B. Note that this threshold has to be larger than the noise level of the aircut motion, and it also has to be small enough so that the depth of contact does not exceed the finishing allowance. Moreover, 4 times the standard deviation shall include 99.994% of the data, i.e., the reliability is high. For these reasons, $\eta + 4\kappa$ is chosen as the threshold. The intersecting point between the fit line and the horizontal line of the mean value η is calculated, which is shown as point C in Fig. 3.6. Consequently, this moment is identified to be the calculated contact time. From the position signal of the feed axis servo, the coordinate of the contact point is obtained. Note that the rising signal of the section A-B is fit as a linear function here considering that the fitting range is small.

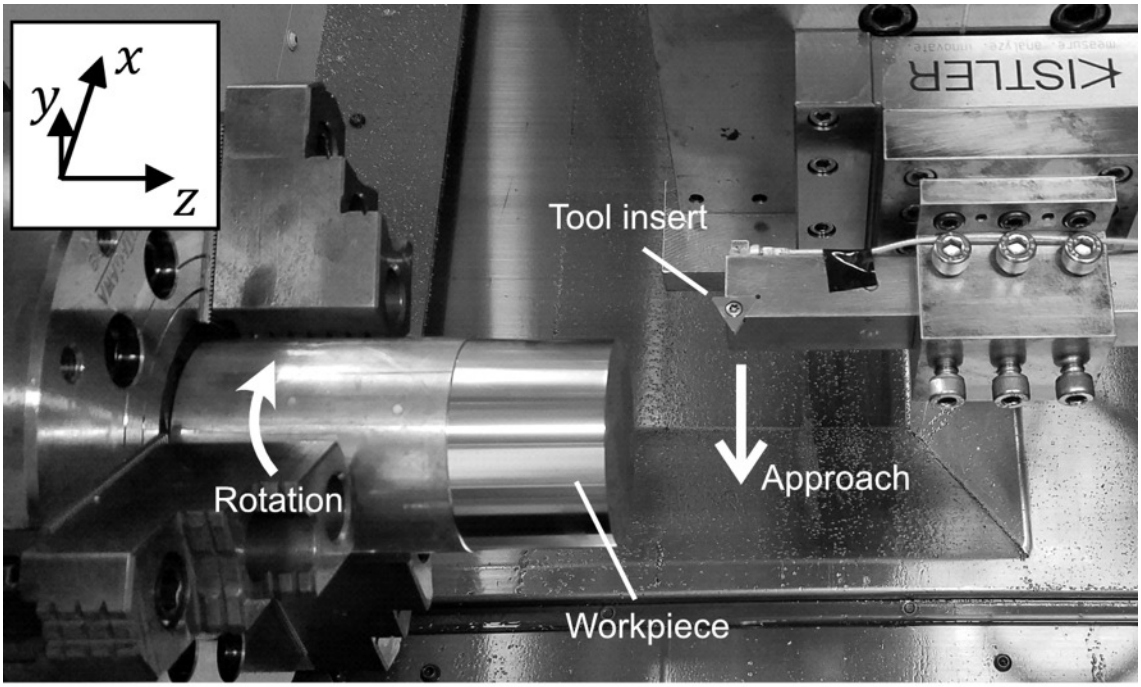

Fig. 3.4. Experimental setup.

Table 3.1. Experimental conditions.

Workpiece properties	
Workpiece material	Brass CuZn39Sn1
Workpiece diameter	(i) 68 (contact detection) (ii) 62 mm (rotational center identification)
Tool properties	
Tool material	HTi10 coated carbide
Nose radius of tool	0.8 mm
Rake / clearance angle of tool	0 / 7 deg
C axis rotational speed	24 min-1
X axis approaching speed (X axis approaching feed rate) Maximum depth of cut	244.8 mm/min (10.2 mm/rev) 0.1 mm
Sampling rate	100 kHz
Number of samples for moving average	100

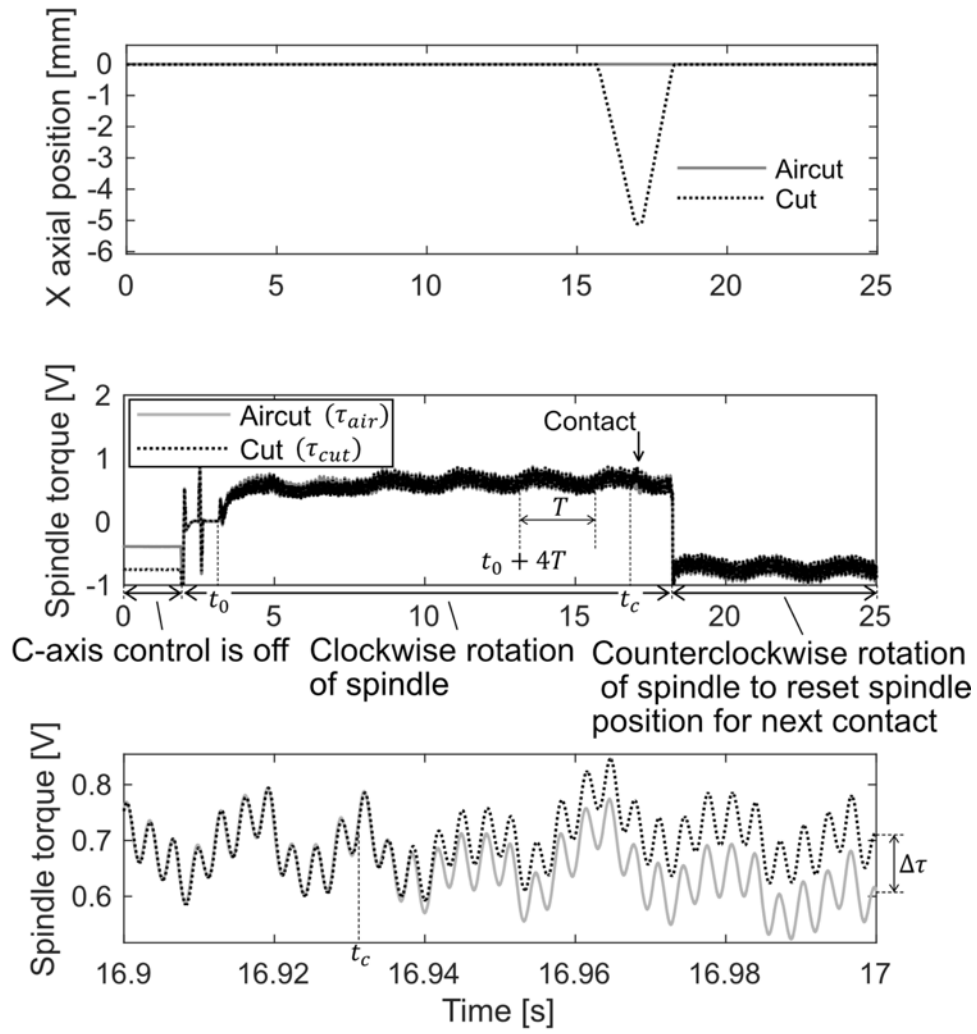

Fig. 3.5. (a) X-axis position signals, (b) spindle torque command signals, and (c) magnified view of spindle torque command signals.

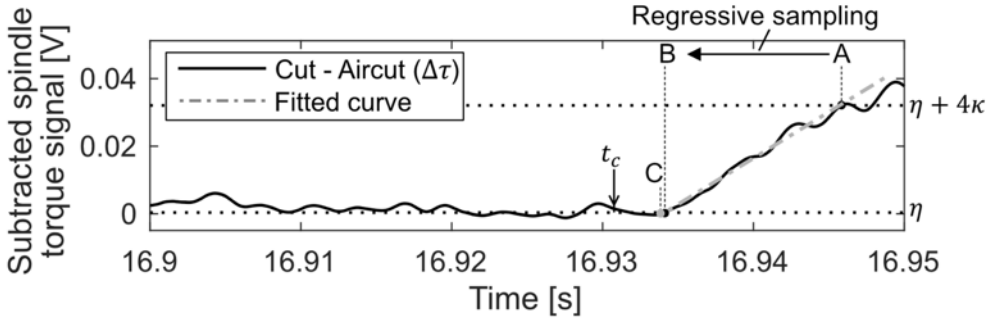

Fig. 3.6. Example of signal processing method.

3.3.3 Gauss-Newton method for identification of workpiece profile

Given that the coordinates of the multiple contact points on the pre-machined surface are extracted from the results of the contact detection method, the coordinates of the rotational center (x_c, y_c) and the diameter D of the workpiece are identified using an iterative algorithm based on the nonlinear least-squares optimization, the Gauss-Newton algorithm. Consequently, the rotational center and the diameter of the workpiece are obtained.

3.4 Results and discussions

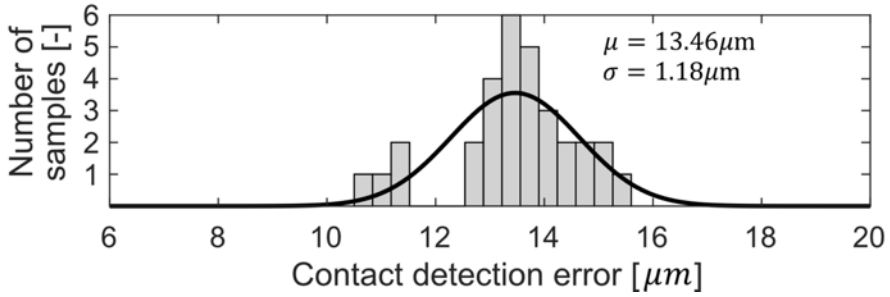

Fig. 3.7. Results of contact detection experiments.

Figure 3.7. shows the histogram of the iterative contact detection experiments with a bin-width of 0.34 μm and the fitted normal distribution. From the results, it can be said that the proposed contact detection method shows repeatability (σ) within a few microns error. Compared to the commercial touch probe sensors for the standard accuracy machine tools, whose repeatability are generally 0.5 μm [81], the proposed method shows a close value without the sensor. However, note that these sensors are only for the information of the workpiece, that is, the tool information will be added to this and become a worse repeatability. The mean value of the contact detection errors (μ) is 13.46 μm. This error originates from the linearization, which refers to the discrepancy between the fitted regression line and the actual curvature of the subtracted signal corresponding to the actual process; e.g., nose radius and cutting-edge radius (which is large if the tool wear is large) affect the process (see Fig. 3.6). Further consideration of these effects is expected to reduce this error at the next step of this research.

Table 3.2 and Fig. 3.8 show the result of the outer diameter turning experiment. It should be noted that the coordinates presented in the table are calculated relatively from the true contact point of the pre-machining process (x_{true}, y_{true}), and this relative coordinate system is common for the contact points and the identified rotational center. Note that the point p_1 is set as the origin of this coordinate system. As shown in the table, the error between the target and measured diameters is 11 μm.

Table 3.2. Result of outer diameter turning experiment.

Relative coordinates of identified contact points on pre-machined workpiece surface	(0, 0), (-0.205, 5), (-1.088, -7) (-3.979, -14), (-8.391, -20)
Identified/measured diameter of pre-machined workpiece	61.968 / 61.980 mm
Relative coordinate of identified rotational center	(-30.972, 1.235)
Target/measured diameter of machined workpiece	60.000 / 60.011 mm

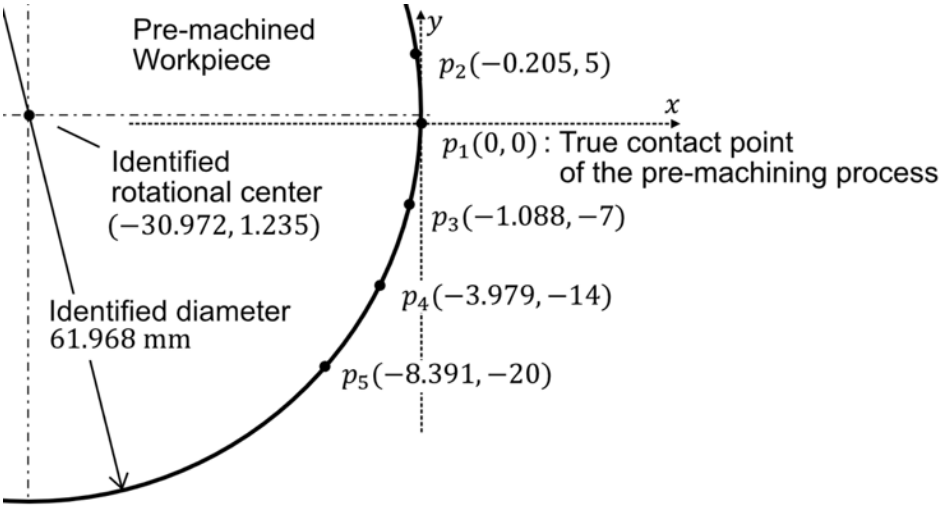

Fig. 3.8. Utilized contact points for identification.

Note that choosing the possibly widest extent of the redundant-axis position range is desirable while considering the tool-edge geometry, i.e., rake/flank angle, for accurate rotational center identification. Also, the identification error can be decreased by increasing the number of contact points utilized for the identification.

3.5 Summary

Two methods for identification of the tool-workpiece relative position, specifically the rotational center, in the general CNC turning process are proposed in this chapter: a novel direct tool-workpiece contact detection method and a rotational center self-identification strategy. The former method identifies the contact coordinates by utilizing the internal data of the machine tool servo. Especially, the servomechanism-originated-error is eliminated by comparing the data of non-contact and contact motion. In addition, the threshold-originated-error is excluded by processing the time-sequential internal data backwardly. The latter method makes multiple tool-workpiece contacts on the pre-machined surface with a redundant-axis movement. The rotational center is identified from those contacts by fitting a circle to the identified workpiece coordinates projected in the cross-sectional direction. Experiments have been carried out to confirm the validity of the proposed methods. The results showed that the proposed methods can realize good accuracy and repeatability, i.e., error of 13.46 μm and repeatability of 1.18 μm for the contact detection and error of 11 μm for the rotational center identification. For future work, the author expect that the proposed self-identification concept can be utilized in further applications such as identification of centers of rotational tables of 5-axis milling machines, perpendicularity between machine tool axes, and so on.

Chapter 4

Conclusions

For the high efficiency cutting process on machine tools, attempts to apply the concept of smart manufacturing to the machining process have been made. In this manner, studies to resolve problems that exist in the machining operation are conducted relying on information achieved from the cutting process. Despite the fact that deep theoretical understandings have been achieved, and a sufficient number of countermeasures have been proposed as outcomes of previous studies, the industrial application has been limited because the necessary cutting-relevant information is often complicated and cost-consuming to be achieved/analyzed. To overcome these limitations and realize practical smart solutions, research on self-identification methods of cutting-relevant information is carried out. The aims of this thesis are to propose real-time self-identification methods of the DOCs and runout for the square end milling process, and to propose the tool-workpiece relative position identification method for the general turning process. The main contributions and findings are summarized as follows:

In Chapter 2, a novel integrated real-time monitoring method for the DOCs and the tool runout based on the frequency domain analysis of the cutting torque for the square end milling process is proposed. The notch frequency due to the helix of the tool is searched from the shape of the tooth passing frequency harmonics, and the ADOC is calculated from it first. For the next step, the RDOC is calculated using the monitored ADOC value from the ratio and phase difference between the tooth-passing frequency components of the cutting torque. With the monitored ADOC and RDOC values, the specific cutting force and the tool runout are calculated from the tool-runout-independent and tool-runout-dependent frequency components, respectively. Finally, an index for evaluating the reliability of the monitored outputs is calculated. Experiments are conducted to confirm the validity of

the proposed method. The desired parameters, i.e., the DOCs and the tool runout, are monitored from the z-axial cutting force, which is proportional to the cutting torque. 3 types of the cutting conditions, i.e., tool paths with constant ADOC and constant RDOC, constant ADOC and changing RDOC, and changing ADOC and constant RDOC, are tested. As a result, the DOCs and the tool runout are monitored successfully even for the transient conditions where the tool enters/exits the workpiece. The computation time is below the machining operation time; therefore, the real-time monitoring system can be realized. In addition, the relationship between the suggested reliability index and the relative errors of the DOCs is investigated. The index is shown to be correlated with the monitoring error of the DOCs; therefore, it can be said that the introduced index indicates the reliability of the monitored parameters.

In Chapter 3, two methods for identification of the tool-workpiece relative position, specifically the rotational center, in the general CNC turning process are proposed: a novel direct tool-workpiece contact detection method and a rotational center self-identification strategy. The former method identifies the contact coordinates by utilizing the internal data of the machine tool servo. Especially, the servomechanism-originated-error is eliminated by comparing the data of non-contact and contact motion. In addition, the threshold-originated-error is excluded by processing the time-sequential internal data backwardly. The latter method makes multiple tool-workpiece contacts on the pre-machined surface with a redundant-axis movement. The rotational center is identified from those contacts by fitting a circle to the identified workpiece coordinates projected in the cross-sectional direction. Experiments have been carried out to confirm the validity of the proposed methods. The results showed that the proposed methods can realize good accuracy and repeatability, i.e., an error of 13.46 μm and repeatability of 1.18 μm for the contact detection and an error of 11 μm for the rotational center identification.

References

[1] Klancnikk S, Senveter J. Computer-based workpiece detection on CNC milling machine tools using optical camera and neural networks. Advances in Production Engineering & Management. 2010 May 1:59-68.

[2] Quintana G, Ciurana J. Chatter in machining processes: A review. International Journal of Machine Tools and Manufacture. 2011 May 1;51(5):363-76.

[3] Munoa J, Beudaert X, Dombovari Z, Altintas Y, Budak E, Brecher C, Stepan G. Chatter suppression techniques in metal cutting. CIRP Annals. 2016 Jan 1;65(2):785-808.

[4] Nath C. Integrated tool condition monitoring systems and their applications: a comprehensive review. Procedia Manufacturing. 2020;48:852-863.

[5] Altintas Y. Manufacturing Automation. Cambridge University Press. 2012.

[6] Davis J, Edgar T, Porter J, Bernaden J, Sarli M. Smart manufacturing, manufacturing intelligence and demand-dynamic performance. Computers & Chemical Engineering. 2012;47:145-156.

[7] Zheng P, Sang Z, Zhong R, Liu Y, Liu C, Mubarok K, Xu X. Smart manufacturing systems for Industry 4.0: Conceptual framework, scenarios, and future perspectives. Frontiers of Mechanical Engineering. 2018;13(2):137-150.

[8] Lu Y, Liu C, Kevin I, Wang K, Huang H, Xu X. Digital Twin-driven smart manufacturing: Connotation, reference model, applications and research issues. Robotics and Computer-Integrated Manufacturing. 2020;61:101837.

[9] ISO 10303-242, Industrial Automation Systems and Integration–Product Data Representation and Exchange–Part 242: Application Protocol: Managed Model-Based 3D Engineering. International Organization for Standardization (ISO) Geneva, Switzerland, 2014.

[10] ISO/AWI 23247, Digital Twin manufacturing framework. Available: https://www.iso.org/standard/75066.html [Accessed April 8, 2018].

[11] Jeon B, Yoon J, Um J, Suh S. The architecture development of Industry 4.0 compliant smart machine tool system (SMTS). Journal of Intelligent Manufacturing. 2020;31(8):1837-1859.

[12] Liu C, Vengayil H, Zhong R, Xu X. A systematic development method for cyber-physical machine tools. Journal of manufacturing systems. 2018;48:13-24.

[13] Cai Y, Starly B, Cohen P, Lee Y. Sensor data and information fusion to construct digital-twins virtual machine tools for cyber-physical manufacturing. Procedia manufacturing. 2017;10:1031-1042.

[14] Altıntas Y, Shamoto E, Lee P, Budak E. Analytical prediction of stability lobes in ball

end milling. Journal of Manufacturing Science and Engineering. 1999;121(4):586-592.
[15] Hahn R. Metal-cutting chatter and its elimination. Transactions of the American Society of Mechanical Engineers. 1953;75(6):1073.
[16] Doi S, Kato S. Chatter vibration of lathe tools. American Society of Mechanical Engineers. 1955.
[17] Tobias S, Fishwick W. The chatter of lathe tools under orthogonal cutting conditions. Transactions of the American Society of Mechanical Engineers, 1958;80(5):1079-1087.
[18] Tobias SA, Fishwick W. Theory of regenerative machine tool chatter. The engineer. 1958;205(7):199-203.
[19] Altintas Y, Weck M. Chatter stability of metal cutting and grinding. CIRP annals. 2004;53(2):619-42.
[20] Tlusty J. Manufacturing Processes and Equipment. Prentice Hall. 2000.
[21] Arnold R. Cutting tools research: report of subcommittee on carbide tools: the mechanism of tool vibration in the cutting of steel. Proceedings of the institution of mechanical engineers. 1946;154(1):261-84.
[22] Hayasaka T, Jung H, Azuma K, Shamoto E. Consolidated chatter stability prediction model considering material removing and ploughing processes. Precision Engineering. 2019;59:120-33.
[23] Dombovari Z, Stepan G. The effect of helix angle variation on milling stability. Journal of Manufacturing Science and Engineering. 2012;134(5):051015.
[24] Otto A, Radons G. Frequency domain stability analysis of milling processes with variable helix tools. In9th International Conference on High Speed Machining 2012 Mar 7.
[25] Altintas Y, Engin S, Budak E. Analytical stability prediction and design of variable pitch cutters. Journal of Manufacturing Science and Engineering. 1999;121(2):173-178.
[26] Tarng YS, Kao JY, Lee EC. Chatter suppression in turning operations with a tuned vibration absorber. Journal of materials processing technology. 2000;105(1-2):55-60.
[27] Marui E, Ema S, Hashimoto M, Wakasawa Y. Plate insertion as a means to improve the damping capacity of a cutting tool system. International Journal of Machine Tools and Manufacture. 1998;38(10-11):1209-20.
[28] Tlusty J, Polacek M. The stability of the machine tool against self-excited vibration in machining. International Research in Production Engineering, Pittsburgh, ASME. 1963;465-474.
[29] Merritt H. Theory of self-excited machine-tool chatter: Contribution to machine-tool chatter research-1. Journal of Manufacturing Science and Engineering. 1965;87(4): 447-454.
[30] Chandiramani N, Pothala T. Dynamics of 2-dof regenerative chatter during turning.

Journal of sound and vibration. 2006;290(1-2):448-64.
[31] Dassanayake A, Suh C. On nonlinear cutting response and tool chatter in turning operation. Communications in Nonlinear Science and Numerical Simulation. 2008;13(5):979-1001.
[32] Altintas Y, Budak E. Analytical prediction of stability lobes in milling. CIRP annals. 1995;44(1):357-62.
[33] Hayasaka T, Ito A, Shamoto E. Generalized design method of highly-varied-helix end mills for suppression of regenerative chatter in peripheral milling. Precision Engineering. 2017;48:45-59.
[34] Suzuki N, Ikada T, Hino R, Shamoto E. Comprehensive Study on Milling Conditions to Avoid Forced/ Self-Excited Chatter Vibrations. Journal of the Japan Society for Precision Engineering. 2009;75(7);908-14.
[35] Inigo B,Colinas-Armijo N, de Lacalle L, Aguirre G. Digital twin-based analysis of volumetric error mapping procedures. Precision Engineering. 2021;72:823-836.
[36] McKeown P. Some aspects of the design of high precision measuring machines. 1975.
[37] Sartori S, Zhang G. Geometric error measurement and compensation of machines. CIRP annals, 1995;44(2):599-609.
[38] Schwenke H, Knapp W, Haitjema H, Weckenmann A, Schmitt R, Delbressine F. Geometric error measurement and compensation of machines—an update. CIRP annals. 2008;57(2):660-675.
[39] Kunzmann H, Trapet E, Wäldele F. A uniform concept for calibration, acceptance test, and periodic inspection of coordinate measuring machines using reference objects. CIRP annals. 1990;39(1):561-564.
[40] ISO 230-1:1996, Test Code for Machine Tools. Part 1. Geometric Accuracy of Machines Operating Under No-Load or Finishing Conditions, ISO, Geneva.
[41] Smith S, Tlusty J. Stabilizing Chatter by Automatic Spindle Speed Regulation. CIRP Annals. 1992;41:433-436.
[42] Budak E, Altintas Y. Analytical Prediction of Chatter Stability in Milling—Part II: Application of the General Formulation to Common Milling Systems. Journal of Dynamic Systems, Measurement, and Control. 1998;120(1):31-36.
[43] Hayasaka T, Ito A, Shamoto E. Generalized design method of highly-varied-helix end mills for suppression of regenerative chatter in peripheral milling. Precision Engineering. 2017;48:45-59.
[44] Hayasaka T, Xu Y, Jung H, Shamoto E, Xu L. Regenerative chatter by teeth allocated in the cutting direction with position-dependent modal displacement ratios, CIRP Annals. 2019;68:409-412.
[45] Tarng Y, Shyur Y. Identification of radial depth of cut in numerical control pocketing routines. International Journal of Machine Tools and Manufacture. 1993;33(1):1-11.

[46] Prickett P, Siddiqui R, Grosvenor R. The development of an end-milling process depth of cut monitoring system. The International Journal of Advanced Manufacturing Technology. 2011:52(1);89-100.

[47] Gaja H, Liou F. Automatic detection of depth of cut during end milling operation using acoustic emission sensor, The International Journal of Advanced Manufacturing Technology. 2016;86(9):2913–2925.

[48] Altintas Y, Yellowley I. The identification of radial width and axial depth of cut in peripheral milling. International Journal of Machine Tools and Manufacture. 1987;27(3):367-381.

[49] Tarn J, Tomizuka M. On-line monitoring of tool and cutting conditions in milling. Journal of engineering for industry. 1989;111:206-212.

[50] Choi J, Yang M. In-process prediction of cutting depths in end milling. International Journal of Machine Tools and Manufacture. 1999;39(5):705-721.

[51] Yang L, DeVor R, Kapoor S. Analysis of force shape characteristics and detection of depth-of-cut variations in end milling. Journal of Manufacturing Science and Engineering. 2005;127(3):454-462.

[52] Leal-Muñoz E, Diez E, Perez H, Vizan A. Identification of the Actual Process Parameters for Finishing Operations in Peripheral Milling. Journal of Manufacturing Science and Egineering. 2018;140(8):084502.

[53] Matsubara A, Soichi I. Monitoring and control of cutting forces in machining processes: a review. International Journal of Automation Technology. 2009;3(4):445-456.

[54] Aggarwal S, Nešić N, Xirouchakis P. Cutting torque and tangential cutting force coefficient identification from spindle motor current. The International Journal of Advanced Manufacturing Technology. 2013;65(1):81-95.

[55] Kline W, DeVor R. The effect of runout on cutting geometry and forces in end milling. International Journal of Machine Tool Design and Research.1983;23(2-3):123-140.

[56] Armarego E, Deshpande N. Computerized End-Milling Force Predictions with Cutting Models Allowing for Eccentricity and Cutter Deflections. CIRP Annals 1991;40(1):25-29.

[57] Hekman K, Liang S. In-process monitoring of end milling cutter runout, Mechatronics 1997;7:1-10.

[58] Seethaler R, Yellowley I. The Identification of Radial Runout in Milling Operations. Journal of Manufacturing Science and Engineering. 1999;121:524-531.

[59] Wang J, Zheng C. Identification of cutter offset in end milling without a prior knowledge of cutting coefficients. International Journal of Machine Tools and Manufacture. 2003;43:687-97.

[60] Koenigsberger F, Sabberwal A. An investigation into the cutting force pulsations during milling operations. International Journal of Machine Tool Design and Research.

1961;1:15-33.

[61] Gradišek J, Kalveram M, Weinert K. Mechanistic identification of specific force coefficients for a general end mill. International Journal of Machine Tools and Manufacture. 2003;44:401-414.

[62] Jayaram S, Kapoor S, Devor R. Estimation of the specific cutting pressures for mechanistic cutting force models. International Journal of Machine Tools and Manufacture. 2001;41:265-281.

[63] Budak E, Altintaş Y, Armarego E. Prediction of milling force coefficients from orthogonal cutting data. Journal of Manufacturing Science and Engineering. 1996;118:216-24.

[64] Lee P, Altintaş Y. Prediction of ball-end milling forces from orthogonal cutting data, International Journal of Machine Tools and Manufacture. 1996;36:1059-72.

[65] Liang S, Wang J. Milling Force Convolution Modeling for Identification of Cutter Axis Offset. International Journal of Machine Tools and Manufacture. 1994;34:1177-1190.

[66] Weckenmann A, Estler T, Peggs G, McMurtry D. Probing Systems in Dimensional Metrology. CIRP Annals. 2004;53(2):657–684.

[67] Uekita M, Takaya Y. On-machine dimensional measurement of large parts by compensating for volumetric errors of machine tools, Precision Engineering. 2016;43:200–210.

[68] Kuschmierz R, Davids A, Metschke S, Löffler F, Bosse H, Czarske J, Fischer A. Optical, in situ, three-dimensional, absolute shape measurements in CNC metal working lathes. The International Journal of Advanced Manufacturing Technology. 2016;84(9):2739–2749.

[69] Che J, Ratnam M. Real-time monitoring of workpiece diameter during turning by vision method. Measurement. 2018;126:369–377.

[70] Shiraishi M, Sumiya H, Aoshima S. In-process diameter measurement of turned workpiece with curvatures by using sensor positioning. Journal of Manufacturing Science and Engineering. 2006;128(1):188–193.

[71] Fan K, Chao Y. In-process dimensional control of the workpiece during turning. Precision Engineering. 1991;13(1):27–32.

[72] Vacharanukul K, Mekid S. New real-time non-contact probe using Gaussian convolution smooth technique for in-process inspection. Sensors and Actuators A: Physical. 2008;141(1):20–28.

[73] Bourne K, Jun M, Kapoor S, DeVor R. An acoustic emission-based method for determining contact between a tool and workpiece at the microscale, Journal of Manufacturing Science and Engineering. Transactions of the ASME. 2008;130(3):0311011–0311018.

[74] Min S, Sangermann H, Mertens C, Dornfeld D. A study on initial contact detection for

precision micro-mold and surface generation of vertical side walls in micromachining. CIRP Annals - Manufacturing Technology. 2008;57(1):109–112.

[75] Min S, Lidde J, Raue N, Dornfeld D. Acoustic emission based tool contact detection for ultra-precision machining. CIRP Annals. 2011;60(1):141–144.

[76] Koga T, Hase A, Ninomiya K, Okita K. Acoustic emission technique for contact detection and cutting state monitoring in ultra-precision turning. Mechanical Engineering Journal. 2019;6(4):19-00169-19–00169.

[77] Murakami H, Katsuki A, Sajima T, Uchiyama K, Houda K, Sugihara Y. Spindle with built-in acoustic emission sensor to realize contact detection. Precision Engineering. 2021;70:26–33.

[78] Castaño F, Haber R, del Toro R, Beruvides G. Conductance sensor for micromachining. A case study on monitoring tool-workpiece contact. Proceedings of the IEEE International Conference on Industrial Technology, 2015 June:1422–1426.

[79] Kakinuma Y, Nagakari S. Sensor-less micro-tool contact detection for ultra-precision machine tools utilizing the disturbance observer technique. CIRP Annals - Manufacturing Technology. 2017;66(1):385–388.

[80] Gander W, Golub G, Strebel R. Least-squares fitting of circles and ellipses. BIT Numerical Mathematics. 1994;34(4):558–578.

[81] Renishaw plc, 2020, Probing systems for CNC machine tools, https://www.renishaw.com/media/pdf/en/d4c5ab9c08f34402a560779ac1a65828.pdf, accessed 27 Apr. 2022.

Publications related to the thesis

JOURNAL PAPERS

1. **K. Lee**, T. Hayasaka, S. Nam, and E. Shamoto, Novel rotational center self-identification of machine tool by utilizing multiple tool-workpiece contacts with redundant-axis movement, *Precision Engineering*, Vol. 77, pp. 185-189, (2023).
2. **K. Lee**, T. Hayasaka, and E. Shamoto, Novel real-time monitoring method of depths of cut and runout for milling process utilizing FFT analysis of cutting torque, *Precision Engineering*, accepted, (2023).

INTERNATIONAL CONFERENCE (underline indicates presenter)

1. **K. Lee**, H. Jung, S. Nam, T. Hayasaka, and E. Shamoto., Novel machining-relevant data acquisition method by tool-workpiece contact detection utilizing servo data of machine tool, *9th International conference on Virtual Machining Process Technology,* Waterloo, Canada, (2020). (After extended abstract was accepted, conference was cancelled due to the COVID-19 pandemic.)

Other publications

INTERNATIONAL CONFERENCES (underlines indicate presenters)

1. S. Nam, **K. Lee**, T. Hayasaka, and E. Shamoto, One-dimensional chatter stability analysis and simplified FRF measurement for three dimensional cutting, *The 20th Machining Innovations Conference for Aerospace Industry* (MIC 2020), Dec. 2, Garbsen, Germany, (2020).
2. H. Jung, **K. Lee**, T. Hayasaka, E. Shamoto, H. Ishii, T. Ueyama, and S. Hamada, Proposal of Ultrasonic Multi-Mode Vibration Cutting for High-Efficiency Surface Texturing, *International Symposium on Precision Engineering and Sustainable Manufacturing*, Jul. 10-13, Da Nang, Vietnam, (2019).

Acknowledgements

First of all, I would like to express my sincere gratitude and appreciation to my research supervisor, Dr. Eiji Shamoto for his priceless guidances throughout this thesis work. His passion toward the research has been the inspiration and motivation to me and has changed my attitude toward the research. His valuable advice enabled me to progress in my research projects and enlightened me. Moreover, I have learned not only the extensive knowledge but also the fundamental attitude and the way of thinking as a researcher and an engineer. The lessons and experiences learned from his teaching will be the firm foundation in my future life.

Next, I would like to express my deep gratitude to Dr. Takehiro Hayasaka for his valuable advice not only on conducting the research projects but also my private life. Whenever I asked him for the discussion, he willingly spent his own time to help me. Without his dedication I could not have continued my academic life. Also he has been the role model for me for his intelligence and tenacity.

Besides my advisors, I am grateful to Dr. Hara Susumu, Dr. Fumihiro Itoigawa for their help in writing my thesis. They have helped me brush up on my thesis and gave me essential comments on my research, which helps to think about my research from different perspectives.

I wish to thank Dr. Takeshi Nakamura, Dr. Ryuta Sato and Mr. Yudai Mizutani for their help in my laboratory life and precious comments and discussions in and out of the research. I also would like to thank Mr. Takahiro Sakai, Mr. Akira Isogai, Ms. Rieko Itoh for all their technical supports. Not to mention, I would like to express my sincere thanks to Ms. Tomoko Ishihara, Ms. Megumi Takaya, Ms. Kazue Kasugai and Ms. Reiko Kawai for their kind supports in office procedures needed at the university and also their warming words.

I would like to thank Dr. Hongjin Jung and Dr. Soohyun Nam for their great help both in my laboratory life and private life. They have always been exemplary as a senior in my laboratory, and conversations with them have

inspired me.

My sincere thanks also go to Dr. Atsushi Ito and Mr. Naohiro Asari from Brother Corp. for their participating in discussions on the research projects. Next, I would like to thank Mr. Shunsuke Fujimaki from Okuma Crop. for his dedicated support on the research project.

It is needleless to say that I am thankful to all of my colleagues in the Manufacturing Engineering Research Group for not only sharing their knowledge and experience with me and encouraging me in laboratory life. I particularly would like to thank Mr. Kota Aoyama and Mr. Kensuke Suzuki. They have been inspirational comrades of the doctoral course. Also, I want to thank Mr. Keigo Miyagawa, Mr. Ryohei Ishida, Mr. Shoma Okamoto, Mr. Hiroki Hayashi, Mr. Kentaro Hisanaga, Mr. Nozomi Ota, Mr. Rion Yamaguchi and Mr. Shotarou Kitada. They have been the best fellows in my laboratory life.

Finally, words cannot express the feelings I have for my families. My father Dr. Taero Lee, his exemplary life as a researcher motivated and introduced my first step to the doctoral course and the life as a researcher. My mother Mrs. Myungsook Jung has given me endless supports, unconditional love and limitless devotions. My sisters, Mrs. Kyungmi Lee and Mrs. Kyungjin Lee gave me encouragements and positive beliefs. This endeavor would not have been possible without the supports of my family.